

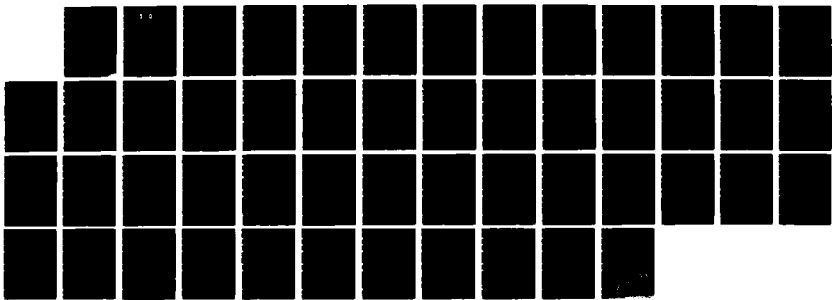
AD-A189 813

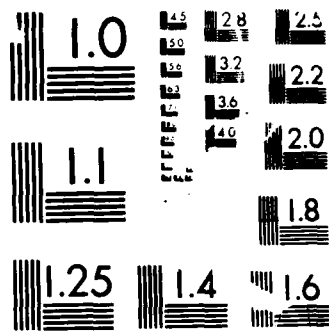
BIMOLECULAR RECTIONS AND ENERGY-TRANSFER PROCESSES OF  
HIGHLY VIBRATIONAL (U) MICHIGAN UNIV ANN ARBOR DEPT OF  
ATMOSPHERIC AND OCEANIC SCIEN J R BARKER DEC 87  
ARO-23199 6-CH DAAG29-85-K-8193 F/G 7/3

1/1

UNCLASSIFIED

NL





MICROCOPY RESOLUTION TEST CHART  
NS-1963-A

2

AD-A189 013

REPORT DOCUMENTATION PAGE

1a. REPORT SECURITY CLASSIFICATION Unclassified		1b. RESTRICTIVE MARKINGS DTIC FILE COPY	
2a. SECURITY CLASSIFICATION AUTHORITY		3. DISTRIBUTION / AVAILABILITY OF REPORT Approved for public release; distribution unlimited.	
2b. DECLASSIFICATION / DOWNGRADING SCHEDULE EXEMPT FEB 03 1988		5. MONITORING ORGANIZATION REPORT NUMBER(S) ARO 23199.6-CH	
4. PERFORMING ORGANIZATION REPORT NUMBER(S) CD		7a. NAME OF MONITORING ORGANIZATION U. S. Army Research Office	
6a. NAME OF PERFORMING ORGANIZATION The University of Michigan	6b. OFFICE SYMBOL (if applicable)	7b. ADDRESS (City, State, and ZIP Code) P. O. Box 12211 Research Triangle Park, NC 27709-2211	
6c. ADDRESS (City, State, and ZIP Code) Ann Arbor, Michigan 48109-2143		9. PROCUREMENT INSTRUMENT IDENTIFICATION NUMBER DAAG29-85-K-0193	
8a. NAME OF FUNDING / SPONSORING ORGANIZATION U. S. Army Research Office	8b. OFFICE SYMBOL (if applicable)	10. SOURCE OF FUNDING NUMBERS	
8c. ADDRESS (City, State, and ZIP Code) P. O. Box 12211 Research Triangle Park, NC 27709-2211		PROGRAM ELEMENT NO.	PROJECT NO.
		TASK NO.	WORK UNIT ACCESSION NO.
11. TITLE (Include Security Classification) BIMOLECULAR REACTIONS AND ENERGY-TRANSFER PROCESSES OF HIGHLY VIBRATIONALLY EXCITED MOLECULES RELATED TO ENERGETIC MATERIALS			
12. PERSONAL AUTHOR(S) BARKER, John R.			
13a. TYPE OF REPORT Final	13b. TIME COVERED FROM 85/7/1 TO 87/9/30	14. DATE OF REPORT (Year, Month, Day) 87/12	15. PAGE COUNT 48
16. SUPPLEMENTARY NOTATION The view, opinions and/or findings contained in this report are those of the author(s) and should not be construed as an official Department of the Army position, unless so designated by other documentation.			
17. COSATI CODES		18. SUBJECT TERMS (Continue on reverse if necessary and identify by block number)	
FIELD	GROUP	SUB-GROUP	
		Multi-photon, infrared absorption, decomposition, laser-induced reactions, infrared emission, energy transfer, Master Equations, Monte Carlo, sums of states, densities of states, anharmonicity.	
19. ABSTRACT (Continue on reverse if necessary and identify by block number)			
<p>Infrared Multiphoton Absorption (IRMPA) was used to produce populations of vibrationally excited 1,1,2-trifluoroethane, which were characterized by optoacoustic measurements of absorbed laser power and collision free decomposition yields. The measurements were accurately fitted with a Master Equation that included Quack's theory of IRMPA, three RRKM unimolecular reaction channels, and collisional energy transfer. The highly constrained adjustable parameters indicate that the optical coupling matrix elements are dramatically reduced in magnitude near reaction threshold energies where vibrational anharmonicity becomes important. Observed infrared fluorescence from the excited molecules is in excellent agreement with Master Equation predictions and it was used to monitor collisional deactivation of the excited molecules. The energy transfer exhibits a weak vibrational energy dependence and no detectable temperature dependence. Experiments were undertaken to ascertain the effect of vibrational energy on bimolecular reactions of TFE, but no such effects have yet been observed.</p> <p>A Monte Carlo method is described for efficient multi-dimensional integration not restricted to hyper-dimensional rectangles, but applied to more complicated domains. When known, the boundaries of an arbitrary integration region can be used to define the sampling domain, resulting in sampling with unit efficiency. For sums of states, the method can include all molecular degrees of freedom, coupled in any fashion. The method is highly efficient and the results show that the off-diagonal anharmonicities produce significant increases in the calculated sum of vibrational states.</p>			
20. DISTRIBUTION / AVAILABILITY OF ABSTRACT <input type="checkbox"/> UNCLASSIFIED/UNLIMITED <input type="checkbox"/> SAME AS RPT <input type="checkbox"/> DTIC USERS		21. ABSTRACT SECURITY CLASSIFICATION Unclassified	
22a. NAME OF RESPONSIBLE INDIVIDUAL		22b. TELEPHONE (Include Area Code)	22c. OFFICE SYMBOL



**BIMOLECULAR REACTIONS AND ENERGY-TRANSFER PROCESSES  
OF HIGHLY VIBRATIONALLY EXCITED MOLECULES RELATED TO  
ENERGETIC MATERIALS**

**FINAL REPORT**

**John R. Barker**

**December 1987**

**U. S. Army Research Office**

**Contract Number DAAG29-85-K-0193**

**The University of Michigan**

**Approved for Public Release;**

**Distribution Unlimited**

Accession For	
NTIS CRA&I	<input checked="" type="checkbox"/>
DTIC TAB	<input type="checkbox"/>
Unannounced	<input type="checkbox"/>
Justification	
By	
Distribution /	
Availability Codes	
Dist	Avail and/or Special
A-1	



## Abstract

Infrared Multiphoton Absorption (IRMPA) was used to produce populations of vibrationally excited 1,1,2-trifluoroethane, which were characterized by optoacoustic measurements of absorbed laser power and collision free decomposition yields. The measurements were accurately fitted with a Master Equation that included Quack's theory of IRMPA, three RRKM unimolecular reaction channels, and collisional energy transfer. The highly constrained adjustable parameters indicate that the optical coupling matrix elements are dramatically reduced in magnitude near reaction threshold energies where vibrational anharmonicity becomes important. Observed infrared fluorescence from the excited molecules is in excellent agreement with Master Equation predictions and it was used to monitor collisional deactivation of the excited molecules. The energy transfer exhibits a weak vibrational energy dependence and no detectable temperature dependence. Experiments were undertaken to ascertain the effect of vibrational energy on bimolecular reactions of TFE, but no such effects have yet been observed.

A Monte Carlo method is described for efficient multi-dimensional integration not restricted to hyper-dimensional rectangles, but applied to more complicated domains. When known, the boundaries of an arbitrary integration region can be used to define the sampling domain, resulting in sampling with unit efficiency. For sums of states, the method can include all molecular degrees of freedom, coupled in any fashion. The method is highly efficient and the results show that the off-diagonal anharmonicities produce significant increases in the calculated sum of vibrational states.

## Contents

Introduction	4
Population Distribution	5
Energy Transfer	6
Bimolecular Reactions	7
Theoretical Work	9
Conclusions	11
Scientific Personnel Supported by ARO	12
Publications Supported by ARO	12
Presentations Based on ARO-Supported Work	13
References	15
Appendix A: Vibrationally excited populations from IR-multiphoton absorption. I. Absorbed energy and reaction yield measurements	
Appendix B: Vibrationally excited populations from IR-multiphoton absorption. II. Infrared fluorescence measurements	
Appendix C: Vibrationally Excited Populations from IR-Multiphoton Absorption. 3. Energy Transfer between 1,1,2-Trifluoroethane and Argon	
Appendix D: Sums of Quantum States for Nonseparable Degrees of Freedom. Multidimensional Monte Carlo Integration	

## Introduction

Energetic materials that combine high performance with low sensitivity have long been sought. Unfortunately, many problems are associated with such materials, including irregular burning, premature detonation, and toxicity. Accidental initiation of materials with inherent molecular sensitivity has been one of the most persistent and formidable problems. This serious problem motivates much research on how energetic material sensitivity and performance are related to the molecular properties of the ingredients.<sup>1</sup> Despite much work on the relationships connecting performance and sensitivity to molecular properties, the detailed reaction sequences leading to detonation are not fully understood.<sup>2</sup> Other factors, such as aging and environmental conditioning (even hydrogen bonding<sup>3</sup>), further complicate the picture, because they can significantly alter the sensitivity of energetic materials.

The focus of the ARO-supported work carried out in this laboratory has been to investigate the fundamental properties of highly vibrationally excited molecules (HVEMs) related to energetic materials. Vibrational excitation is produced in all high temperature systems, including the extremely hostile environments associated with energetic material combustion, detonation, and deflagration. Little is known about the energy transfer properties, spectroscopy, and chemical reactions of highly vibrationally excited molecules. It is possible that HVEMs may exhibit enhanced bimolecular reaction rates and unusual chain branching reactions.

In this project, we have used a prototype molecule to investigate methods for preparing HVEMs and characterizing their population distributions. This phase of work has been very successful and we have completed perhaps the most detailed analysis ever carried out on preparation of HVEMs by infrared multiphoton absorption (IRMPA). In addition, we used the HVEMs prepared by

IRMPA to determine the vibrational energy transfer properties of the HVEMs. At present, we are engaged in a search (so far unsuccessful) for vibrational enhancement of bimolecular reactions.

Infrared multiphoton absorption (IRMPA) is a powerful method for producing large populations of HVEMs through the use of a high power CO<sub>2</sub> laser. During the excitation process, some molecules absorb many photons, while other molecules only absorb a few, resulting in broad population distributions controlled by the laser fluence. The first necessity was to develop methods for determining the population distributions.

### Population Distribution

To determine the population distribution, we first selected a particularly favorable prototype molecule (1,1,2-trifluoroethane, i.e. "TFE") and used a combination of experimental techniques in conjunction with a detailed Master Equation model, as summarized in Appendix A. The basic idea was to take several experimental measures of the population distribution, fit the observations with a single theoretical model, and then use the model to fill in the gaps in our knowledge.

The first experimental measure was the average amount of energy absorbed from the laser; this gives the average energy of the population distribution. The second experimental measure was the decomposition yield as a function of laser fluence. Because only the most chemically energetic molecules decompose, this was a measure of the high energy tail of the distribution. The Master Equation model included collisions, optical pumping, stimulated emission, IRF, three RRKM unimolecular reaction channels, etc. and it was possible to fit the data with relatively little empiricism, as described in Appendix A.

To test the accuracy of the population distribution as described with the Master Equation, we carried out infrared emission

experiments in which we determined the IRF intensity from the C-H modes as a function of laser fluence, which determines the population distributions. As shown in Appendix B, a comparison between the experiments and IRF intensities predicted by the Master Equation model showed excellent agreement, demonstrating that the combination of techniques and the Master Equation model gave accurate population distributions.

### Energy Transfer

The first application of the population distributions was the determination of the energy transfer properties of TFE, the prototype molecule, in collisions with argon, as described in Appendix C. In these experiments, IRF from TFE was monitored as a function of time. The intensity was observed to decay with time constants that depended on laser fluence and on the gas mixture composition. High laser fluences produce initial populations with higher excitation, and the final temperature is governed by the relative amount of TFE in the gas mixture. Thus, by varying the gas composition and laser fluence independently, we were able to determine the dependence of  $\langle \Delta E \rangle_d$  (the average energy lost in deactivating collisions) on both excitation energy and bath temperature. This was the first such measurement using TFE and the results appear to be quite reasonable, when compared with similar molecules.

A continuation of the energy transfer experiments is currently underway. Our objective here is to compare the time-resolved optoacoustic technique used by Gordon and coworkers to the IRF method mentioned above. This method is related to time-dependent thermal lensing and is one of several photothermal techniques that can be applied to energy transfer. In essence, the energy transfer produces rapid heating from the deposited laser energy. The heating produces a compression wave that travels outward from the laser beam. Associated with the compression wave is an expansion wave with amplitude dependent on the rate of V-T energy transfer; thus

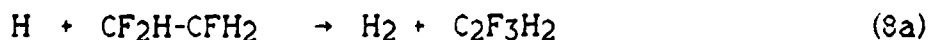
the ratio of the wave amplitudes is related to the time constant for energy transfer. Either the theory of Bailey et al., or the more complete theory of Barker and Rothem can be used to describe the pressure waves in this energy transfer system.

### Bimolecular Reactions

We have expended a major effort over the past year to detect and measure changes in bimolecular reactivity of TFE due to vibrational excitation. In these experiments, we have attempted to observe the reactions of H-atoms and O-atoms with IRMPA-excited TFE. So far, we have observed no enhancement, but we plan to make several more attempts, before concluding the experiments.

Before beginning the experiments on bimolecular reactions, we first tested our new laboratory laser (Lumonics Hyperex 400) to determine whether it produces populations similar to those produced by the Tachisto and Lumonics 103 lasers originally used by us at SRI. New optoacoustic measurements were within 10% of the original data, and decomposition yield measurements were also reproduced within the experimental uncertainties (3% yield, compared with 4% yield obtained earlier at  $0.9 \text{ J cm}^{-2}$ ). These levels of agreement are surprisingly good, because the new measurements were carried out with a different laser, new power meter, different optoacoustic microphone, and new quadrupole mass spectrometer.

The reaction that we are currently investigating is that of H-atoms with TFE to produce  $\text{H}_2$  and  $\text{HF}$ :



We estimate that both reaction channels have A-factors of about  $10^{10} \text{ cm}^3 \text{ s}^{-1}$  and activation energies of about 340 to 400  $\text{kJ mol}^{-1}$

and we are in the process of measuring the thermal rate constants to confirm these estimates.

If vibrational energy is important in the reaction, it may increase (or decrease!) the total reactivity of TFE and/or modify the branching ratio for the two channels. H-atoms (or O-atoms) are produced with a microwave discharge in a flowing argon or helium carrier gas; the atom concentration is determined by titration with NO<sub>2</sub> (the end-point is determined mass spectrometrically):



This reaction is followed by several subsequent reactions, giving a stoichiometry factor somewhat larger than unity.

The actual H-atom (or O-atom) concentration is needed only when using H-atom-rich conditions, as we have attempted to do, thus far. Unfortunately, we have not been able to produce sufficient concentration of H-atoms under the low pressure conditions needed to avoid collisional deactivation of the excited molecules. Under these conditions, we also measured the reaction rate of H-atoms with ethylene to verify the H-atom concentrations. This experiment showed an even lower [H], indicating that NO<sub>2</sub> was probably also being lost due to photolysis from the microwave discharge.

To avoid these problems, we must use TFE-rich conditions, where the concentration of vibrationally excited TFE is in great excess over [H]. These conditions are also desirable for another reason. H-atoms are likely to deactivate rapidly the excited TFE, and the low [H] will reduce the importance of this process (we plan to measure this deactivation rate). A major advantage of infrared multiphoton absorption is that it is relatively easy to produce large concentrations of vibrationally excited molecules. By using 30 mTorr of TFE, we will produce  $\approx 10^{15} \text{ cm}^{-3}$  excited TFE molecules, much larger than the  $\approx 10^{13} \text{ cm}^{-3}$  H-atoms we are currently producing. To work with low [H], we will use resonance absorption and/or resonance fluorescence at the Lyman- $\alpha$  line in future experiments.

Despite the low H-atom concentrations, we have carried out experiments by using mass spectrometry to monitor [TFE] and the production of reaction products. Thus far, we have not observed any significant variation due to bimolecular reaction in the HF production, or in loss of TFE when the molecule is irradiated at moderate fluences. These results have been disappointing, but not exceptional, since our conditions have not been optimal. Moreover, some polyatomic reaction systems have shown a dependence on vibrational energy, but others have not.<sup>4</sup> Our experiments are still underway, and monitoring H-atom concentrations in the presence of excess [TFE(vib)] is likely to be a more sensitive way of observing changes in the reaction rate. Regardless of whether an effect is ultimately observed, such experiments could not even be attempted without IRMPA production of excited molecules.

### Theoretical Work

As part of the analysis of the population distributions, a full Master Equation treatment was needed. Although much of the computer code had already been written, we found it necessary to include M. Quack's statistical-dynamical theory of infrared multiphoton excitation, as described in Appendix A. Although most of the implementation of this theory was straightforward, we eliminated many of the approximations that were originally used by Quack. For example, we used exact counts of vibrational states, rather than the semiclassical approximations used by the original authors.

In addition to the implementation of Quack's theory, we also have carried out original research on the sums and densities of states of HVEMs (Appendix D). In real molecules, all degrees of freedom (DOF) are coupled, as distinguished from the usual separable harmonic and anharmonic models. For separable DOF, the sums and densities of states are easily counted exactly, through use of the Stein-Rabinovitch algorithm. However, when molecules are highly

excited, separability breaks down and coupling among the DOF becomes dominant. Our research on molecules with coupled DOF was motivated by the need to determine exact densities of states for HVEMs.

To treat coupling among all DOF is a major challenge, because the couplings include the usual diagonal and off-diagonal vibrational anharmonicities, couplings between vibrations and rotations, coriolis effects, Fermi resonances, etc. For different theoretical applications different ones of these couplings may be of interest. Our approach was to develop a Monte Carlo method for treating these systems, because such methods are, in principle, completely general.

The Monte Carlo method we developed is, we believe, a new approach to multi-dimensional integration. We employed it in discrete state-space for the purpose of counting sums of states, but it can also be used with continuous variables. The details are given in Appendix D.

To demonstrate the calculation of sums of states for non-separable DOF, we used the spectroscopic parameters for H<sub>2</sub>O and for CH<sub>2</sub>O to calculate the vibrational sums of states. We used the actual spectroscopic data, not a theoretical model! The results showed that the Monte Carlo method we developed is efficient and practical. The resulting sums of states showed that separable models for the same molecules underestimate the actual sums of states by significant factors, which could affect theoretical interpretations in some cases.

Future work on development of this method will treat couplings between vibrations and rotations, which are crucially important in unimolecular reactions near threshold.

## Conclusions

The completed phases of this research were highly successful. The characterization of the population distribution of excited TFE molecules was probably the most complete ever carried out on any molecule other than SF<sub>6</sub>. The IRF emission test of the distribution function showed excellent agreement with theory, and the IRF was then used to measure energy transfer between excited TFE and argon collider gas.

The difficult experiments to determine the effect of vibrational energy on bimolecular reactions are still underway and no definitive conclusion has been reached, as yet. Using mass spectrometry to monitor TFE concentrations and reaction products, we have not observed any influence of vibrational energy. However, conditions are not optimum, since the H-atom concentrations are too low to provide a good test. We will use Lyman- $\alpha$  photometry and/or resonance fluorescence to monitor H-atom concentration in future experiments. Under these conditions, effects are more likely to be observed.

The theoretical efforts have been very successful, leading to improvements in the collisional/photophysical Master Equation used in analysis of experimental results, as well as in development of a new Monte Carlo multidimensional integration scheme and evaluation of sums of states for coupled vibrational degrees of freedom.

### **Scientific Personnel Supported by ARO**

Professor John R. Barker, Principal Investigator

Dr. Jean-Michel Zellweger, Postdoctoral Research Associate

Dr. Murthy L. Yerram, Postdoctoral Research Associate

Trevor C. Brown, Visitor from The University of Adelaide

### **Publications Supported by ARO**

John R. Barker and Rachel E. Golden, "Temperature-Dependent Energy Transfer: Direct Experiments Using Azulene," *J. Phys. Chem.*, **88**, 1012 (1984).

Trevor C. Brown, Keith D. King, Jean-Michel Zellweger, and John R. Barker, "Experimental Studies of Population Distributions Produced by Infrared Multiphoton Absorption," *Ber. Bunsenges. Phys. Chem.*, **89**, 301 (1985).

Wendel Forst and John R. Barker, "Collisional energy transfer and macroscopic disequilibrium. Application to azulene," *J. Chem. Phys.*, **83**, 124 (1985).

Jean-Michel Zellweger, Trevor C. Brown, and John R. Barker, "Vibrationally excited populations from IR-multiphoton absorption. I. Absorbed energy and reaction yield measurements," *J. Chem. Phys.*, **83**, 6251 (1985).

Jean-Michel Zellweger, Trevor C. Brown, and John R. Barker, "Vibrationally excited populations from IR-multiphoton absorption. II. Infrared fluorescence measurements," *J. Chem. Phys.*, **83**, 6261 (1985).

Jean-Michel Zellweger, Trevor C. Brown, and John R. Barker,  
"Vibrationally Excited Populations from IR-Multiphoton Absorption. 3.  
Energy Transfer between 1,1,2-Trifluoroethane and Argon," J. Phys.  
Chem., **90**, 461 (1986).

John R. Barker, "Sums of Quantum States for Nonseparable Degrees  
of Freedom: Multidimensional Monte Carlo Integration," J. Phys.  
Chem., **91**, 3849 (1987).

J. R. Barker and M. L. Yerram, "Characterization and Exploitation of  
Vibrationally Excited Populations Produced by IRMPA," in  
Multiphoton Processes, ed. S. J. Smith, Cambridge University Press,  
in press.

#### **Presentations Based on ARO-Supported Work**

John R. Barker, Trevor C. Brown, and Keith D. King, "Bimolecular  
Reactions and Energy Transfer Involving Highly Vibrationally  
Excited Molecules", 8th International Symposium on Gas  
Kinetics, University of Nottingham, England, 15 - 20 July 1984  
(Invited).

John R. Barker, Trevor C. Brown, and Keith D. King, "Kinetic Studies  
on Excited Molecule Populations Prepared by Infrared  
Multiphoton Absorption", Meeting on Laser Studies in Reaction  
Kinetics, 24 - 27 July 1984 (Invited).

John R. Barker, Jean-Michel Zellweger, and Trevor C. Brown,  
"Vibrationally Excited Populations from I. R. Multiphoton  
Absorption: Optoacoustic and Reaction Yield Measurements",  
International Conference on Chemical Kinetics, National Bureau  
of Standards, Gaithersburg, Maryland, 17 - 19 July 1985.

John R. Barker, Jean-Michel Zellweger, and Trevor C. Brown,  
"Vibrationally Excited Populations from I. R. Multiphoton  
Absorption: Infrared Fluorescence Measurements", International

Conference on Chemical Kinetics, National Bureau of Standards,  
Gaithersburg, Maryland, 17 - 19 July 1985.

John R. Barker, "Infrared Laser-Produced Populations of Highly  
Excited Molecules", American Chemical Society, 40th Northwest  
Regional Meeting, Sun Valley, Idaho, 19 - 21 June, 1986 (invited).

Jean-Michel Zellweger, Trevor C. Brown, and John R. Barker,  
"Vibrationally Excited Populations from I. R. Multiphoton  
Absorption: Optoacoustic and Reaction Yield Measurements",  
191st American Chemical Society Meeting, New York, 13 - 18  
April, 1986.

Jean-Michel Zellweger, Trevor C. Brown, and John R. Barker,  
"Vibrationally Excited Populations from I. R. Multiphoton  
Absorption: Infrared Fluorescence Measurements", 191st  
American Chemical Society Meeting, New York, 13 - 18 April,  
1986.

John R. Barker, "Sums and Densities of States for Non-separable  
Anharmonic Degrees of Freedom", XVII Informal Conference on  
Photochemistry, Boulder, Colorado, 22 - 26 June 1986.

John R. Barker, Trevor C. Brown, Jean-Michel Zellweger, and Murthy  
L. Yerram, "Characterization and Exploitation of Vibrationally  
Excited Populations Produced by IRMPA", International  
Conference on Multiphoton Processes, Boulder, Colorado, 13 - 17  
June 1987 (invited).

## References

1. D. Price, Chem. Rev., 59, 801 (1959); M. J. Kamlet and S. J. Jacobs, J. Chem. Phys., 48, 23 (1968); A. Delpuech and J. Cherville, Propellants and Explosives, 3, 169 (1978); M. J. Kamlet and H. G. Adolph, Propellants and Explosives, 4, 10 (1979).
2. M. E. Hill and J. M. Guimont, "Desensitization of Explosive Materials", Final Report, Contract N0014-76-C-0810, December 1979.
3. Chem. Eng. News, 65, 25 (1987): article describes work by J. W. Rogers, H. C. Peebles, R. R. Rye, J. S. Binkley, and J. E. Houston.
4. For example, see D. Klenerman and R. N. Zare, Chem. Phys. Letters, 130, 339 (1986); J. Xu, A. R. Slagle, D. W. Setser, and J. C. Ferrero, Chem. Phys. Letters, 137, 63 (1987).

APPENDIX A.

# Vibrationally excited populations from IR-multiphoton absorption. I. Absorbed energy and reaction yield measurements<sup>a)</sup>

Jean-Michel Zellweger

*Department of Chemical Kinetics, Chemical Physics Laboratory, SRI International, Menlo Park, California 94025*

Trevor C. Brown

*Department of Chemical Engineering, University of Adelaide, Box 498, G.P.O., Adelaide, South Australia 5001*

John R. Barker<sup>b)</sup>

*Department of Atmospheric and Oceanic Science, Space Physics Laboratory, University of Michigan, Ann Arbor, Michigan 48109-2143*

(Received 31 July 1985; accepted 6 September 1985)

The molecule 1,1,2-trifluoroethane (TFE) was used in experiments to determine the population distribution of excited molecules produced by infrared multiphoton absorption induced by high power TEA CO<sub>2</sub> lasers operating at 1079.85 cm<sup>-1</sup> [9.6 μm R (22) line]. Optoacoustic measurements of absorbed laser power provided a measure of the mean energy of the population distribution, while very low pressure photolysis measurements of the collision-free decomposition yield gave information about the high-energy tail of the distribution. The experimental results were accurately simulated using a Master Equation model that incorporated Quack's statistical-dynamical theory of infrared multiphoton absorption (cases B and C), RRKM unimolecular reactions (three channels), and collisional energy transfer. The computer simulations included known TFE molecular properties and only four adjustable parameters, which were very highly constrained in order to fit the experimental data. From the simulations, we conclude that the optical coupling matrix elements are dramatically reduced in magnitude for energies above the reaction thresholds. This effect is symptomatic of the vibrational anharmonicity due to the presence of the reaction channels, even in molecules that have not yet reacted, resulting in vibrational frequency shifts of the absorption lines out of resonance with the laser line. This effect is expected to be present and observable in other highly vibrationally excited molecules.

## INTRODUCTION

A little more than ten years ago, great interest was aroused by the first observations of chemical reactions induced by infrared lasers.<sup>1</sup> The observations could only be explained if isolated molecules absorbed many infrared photons, leading to bond fission and molecular elimination reactions. Because not all irradiated molecules absorb the same number of photons, the population distributions are produced with substantial energy dispersions.

Despite the broad population distributions, IR-multiphoton absorption has great potential as a useful laboratory tool because of two features: (1) many molecules absorb light from powerful infrared (e.g., CO<sub>2</sub>) lasers and therefore the effect is general, and (2) almost all irradiated molecules are excited to relatively high vibrational energies. By varying laser power, wavelength, and other parameters, the average energy of the population can be controlled, much as the average energy can be controlled in thermal systems by changing the temperature. Until the population distributions are better characterized, however, the usefulness of IRMPA is limited, despite its potential as a laboratory tool.

Although hundreds of publications have described IRMPA and several excellent reviews have been published,<sup>1</sup>

the details of the population distributions in large molecules are still not well known, but only have been inferred from limited measurements<sup>2,3</sup> and from theoretical calculations. In this paper, two experimental techniques (VLPΦ measurement of decomposition yields<sup>4</sup> and optoacoustic measurement of absorbed laser power<sup>5</sup>) were employed along with a Master Equation theoretical model<sup>6</sup> to obtain improved estimates of the population distributions produced by IRMPA. By using more than one experimental technique, the theoretical modeling is highly constrained, leading to reliable estimates for the population distributions. A third experimental technique, infrared fluorescence spectroscopy, was also applied in this study and it shows excellent consistency with the other techniques, but it has not been independently calibrated and so it is described separately in the following paper.<sup>7</sup>

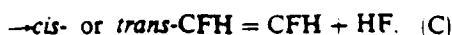
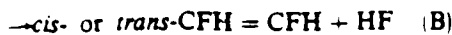
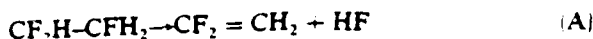
1,1,2-trifluoroethane (TFE) was chosen for the experiments for several reasons:

(1) A vibrational assignment<sup>8</sup> has been made and TFE has a strongly absorbing C-F stretch mode near 1076 cm<sup>-1</sup>, suitable for pumping with a CO<sub>2</sub> laser.

(2) TFE has simple unimolecular reactions (HF molecular eliminations by three reaction pathways), which have already been thoroughly investigated in thermal and chemical activation experiments.<sup>9</sup> These molecular elimination reactions do not lead to secondary chemistry, simplifying interpretation of the results.

<sup>a)</sup> All of the experimental work was carried out at SRI International and was supported by the U.S. Army Research Office.

<sup>b)</sup> Address correspondence to this author.



(3) The internal and external rotations in TFE are relatively massive and they have low symmetry, producing a high density of optically accessible vibrational states, which enhances the efficiency of IRMPA. Moreover, the wide dispersion of the vibrational frequencies produces a "filled-in" density of states, with few regions of low state density, except at very low energy.

(4) The C-H stretch mode frequencies are conveniently separated from the frequencies of other modes in TFE, reducing the spectroscopic resolution requirements in the infrared fluorescence experiments.<sup>7</sup>

(5) The bimolecular reactions of TFE with atoms and simple free radicals are expected to be straightforward and suitable for studies of the effects of vibrational energy on bimolecular reactivity.

The usefulness of TFE has been borne out in the experiments reported here. High IRMPD yields were obtained and the experimental observations were entirely in accord with the qualitative expectations. The results are highly consistent and they lead to better knowledge of the properties of highly vibrationally excited molecules, as described in the following sections.

## EXPERIMENTAL

The VLP  $\Phi$  technique for measurement of collision-free IR multiphoton decomposition (IRMPD) yields has been described elsewhere in detail,<sup>4</sup> except for a few modifications. Gases at low pressure (<20 mTorr) are irradiated in a 2 cm diam by 10 cm long Knudsen cell equipped with KCl windows. The gas escapes through an aperture at a rate dependent only on the mean molecular velocity, the cell volume, and the area of the aperture. In the present experiments, the escape aperture was fabricated from a Teflon-bore greaseless stopcock in order to have continuous control of the residence time. Since the stopcock could not be reproducibly reset to known aperture areas, 1 Torr Baratron capacitance manometer (model 223A) was used to monitor gas pressure in the cell directly. The residence time  $\tau$  is given by<sup>10</sup>

$$\tau = PV_{\text{cell}}N_0/(RTF_A), \quad (1)$$

where  $P$  is the observed pressure,  $V_{\text{cell}}$  is the cell volume,  $N_0$  is Avogadro's number,  $R$  is the gas law constant,  $T$  the temperature, and  $F_A$  is the measured gas flow rate (measured by timing the rate of pressure increase in a calibrated volume); the escape rate constant is  $\tau^{-1}$ .

The composition of the gas escaping from the cell is monitored by a modulated molecular beam mass spectrometer, as described elsewhere.<sup>11</sup> For this purpose, a Finnegan Spectrascan 400 quadrupole mass spectrometer was used with an SRI-built "peak picker" for selection of specific mass peaks. The output of the quadrupole was amplified with a PAR model 181 charge-sensitive preamplifier and the modulated signal was isolated from background with an Ith-

aco model 391 lock-in amplifier, locked to the 200 Hz tuning-fork chopper (Bulova Time Products). For further signal averaging, the output from the lock-in was captured and stored by a Nicolet model 1072 signal averager, which was interfaced with a DEC LSI 11/2 computer for storage of the data on floppy disks and subsequent analysis.

Two CO<sub>2</sub> TEA lasers were used in the experiments: a low repetition rate laser (Lumonics model K103), which can deliver > 5 J/pulse at < 0.25 Hz, and a high repetition rate laser (Tachisto, model 555G), which can deliver < 1 J/pulse at up to 22 Hz. For most experiments, the lasers were operated on the 9.6  $\mu\text{m}$  R(22) line (1079.85 cm<sup>-1</sup>) and, in many experiments, a three-power Gallilean telescope (Janos Technology) was used to concentrate the beam. Laser pulse energy was monitored continuously with a volume-absorbing calorimeter (Scientech, Inc.) connected to a strip-chart recorder. Under our operating conditions, the thyatron-triggered Tachisto laser showed pulse-to-pulse energy variations of about  $\pm 5\%$ , while the older, spark-gap-triggered Lumonics showed variations of more than  $\pm 20\%$ .

Laser fluence was determined by the measured laser pulse energy, divided by the laser beam cross-sectional area. When the telescope was not used, the laser beam cross section was defined by an iris diaphragm positioned before the entrance window. When the beam was concentrated by the telescope, the area was determined by scanning a pinhole in a two-dimensional survey across the beam, and applying the 1/e criterion. The areas so defined were very similar to the patterns produced on thermal printer paper, which was used for quick checks of beam area. Additional confidence in the printer-paper measurements was gained by measuring the beam area before, and after the telescope: within  $\pm 10\%$ , the ratio of the beam areas was 1/9. Laser fluence inside the cell was assumed to equal that measured at the cell entrance, because reflection losses from the entrance window are nearly compensated by back reflections from the exit window and the small residual correction is much less than the estimated  $\pm 30\%$  uncertainty in the absolute fluence.

The laser fluence was varied in crude steps by attenuation with polyethylene films; fine adjustments to the fluence were made by varying the high voltage settings on the laser. At high repetition rates, the polyethylene films were cooled with a stream of compressed air to prevent their deformation and melting.

For both lasers, the far-field pattern had hot and cold zones that differed from the average fluence by 20% to 30%. These patterns depended on laser alignment and optical path from the laser to the cell, but they were somewhat reproducible, and their presence did not seem to affect the results. The overall intensity profile of the beam from each laser was approximately trapezoidal, similar to the profile measured in earlier work.<sup>12</sup>

IRMPD yields were determined using two variations of the VLP  $\Phi$  technique: single-shot accumulation, or fast-repetition quasi-steady-state depletion. The first method has been described previously. The quasi-steady-state depletion method used the fast repetition rate capability of the Tachisto laser to repeat laser shots many times during the gas residence time. Since each parcel of gas was irradiated many

times prior to exiting the cell, larger depletions of reactant gas were generated, allowing measurement of smaller yields-per-shot that could be attained using the single-shot accumulation technique. Tests showed that 1,1-difluoroethylene (the only ethylene reaction product commercially available: PCR, Inc.) does not absorb the laser photons. The reported vibrational frequencies of 1,1-difluoroethylene and of *cis*- and *trans*-1,2-difluoroethylene (the other products) indicate that they will not absorb at the laser wavelength.<sup>13</sup> (Yields were also measured optoacoustically, as described below.)

In the absorbed laser energy experiments, the cell was a Pyrex cylinder (4 cm diam  $\times$  30 cm long) equipped with inlet and outlet stopcocks to facilitate gas flow, and O-ring connectors to accommodate end and side windows and the electrical feedthrough for the electret microphone/preamplifier (Knowles, BT-1759). The output from the microphone/preamplifier was further amplified (Tektronix model AM502) and captured with a transient recorder (Biomation model 805) interfaced to the Nicolet signal averager. By positioning the microphone near the laser beam, the initial acoustic wave generated by the absorbed energy strikes the microphone before the waves reflected from the cell walls can cause interference<sup>5</sup>; thus, only the first maximum in the complex signal was deemed significant. Experiments were repeated (16–256 shots) until a statistical precision of  $\pm 2\%$ – $3\%$  was achieved.

The optoacoustic method was also adapted for measurement of yield vs fluence data at pressures too high for the VLP $\Phi$  technique. The procedure was to introduce a known TFE/argon mixture into the optoacoustic cell and measure the OA signal at a low fluence. The gas mixture was then irradiated for a known number of laser shots at the higher fluence to be investigated; the static gas mixture was depleted by this irradiation. Following irradiation, the OA signal was again measured at low fluence to determine the amount of depletion, from which the IRMPD yield-per-shot was determined, the reaction products (at room temperature) do not interfere by absorption of laser light. Small air leaks limited the durations of data acquisition runs and the lowest pressures attainable, but useful data were obtained, as described in the Results section.

1,1,2-trifluoroethane was obtained commercially (PCR, Inc.) and was used after degassing in a grease-free high vacuum line. Gas purity was checked with a gas chromatograph/mass spectrometer (Varian, Inc.) and the major impurity was found to be 1,1,1-trifluoroethane (about 0.1%).

## RESULTS

### IRMPD yields vs fluence

The two versions of the VLP $\Phi$  technique were used to obtain most of the data on IRMPD yields, but these methods were complemented by the optoacoustic technique, which is suitable for measuring the effect of pressure. High fluence results were obtained using the Lumonics laser and lower fluence measurements were made with the high repetition rate Tachisto laser. At high fluences, the principal source of error was the fluctuation of laser power; long-term drift and instability of the mass spectrometer were the limiting factors at low fluence. The minimum uncertainty achieved with the

single-shot accumulation method corresponds to about  $\pm 2\%$ – $3\%$ , as determined in blank runs. Yields of that order, or lower were not reliably measured using the single-shot accumulation method in our experiments. However, by using the high repetition rate laser, each parcel of gas entering the VLP $\Phi$  cell is irradiated 10–12 times during its residence time, improving the precision of the yield measurements by a factor of 5–10.

The results obtained at  $1079.85\text{ cm}^{-1}$  using both methods and both lasers show very good consistency, even when the laser beam mode structure is deliberately varied. As a test, the area of irradiation was changed from  $2.7$  to  $0.78\text{ cm}^2$ , using the Lumonics laser, and the results were indistinguishable from those obtained using a  $0.42\text{ cm}^2$  beam from the Tachisto. Because of the insensitivity of the results to beam spatial modes, deconvolution<sup>12</sup> of the spatial profile was not attempted, although an iterative approach based on the calculated results would be feasible (and time consuming).

Tests were carried out to eliminate other possible sources of experimental artifacts. For example, the residence time in the cell was held constant at  $0.88\text{ s}$  and the cell pressure was varied from  $0.8$  to  $20\text{ mTorr}$  without significantly affecting the results obtained; at higher pressures, the yields decreased slightly. In another test, the gas flow rate was held constant and the residence time was varied from  $0.10$  to  $0.56\text{ s}$ , without affecting the results.

All of these data are presented in Fig. 1, where the data sets show excellent consistency. The data are plotted on probability graph paper as a log-normal cumulative distribution, because it has been shown that for many IRMPD theoretical models and some experimental data, such a presentation gives straight lines.<sup>14</sup>

The optoacoustic measurements of yield vs fluence were carried out at pressures ranging from  $1.5\text{ mTorr}$  TFE diluted in  $33\text{ mTorr}$  argon, up to pressures as high as  $10\text{ Torr}$ , as presented in Fig. 2. The most extensive optoacoustic data set corresponds to a total pressure of about  $35\text{ mTorr}$ . These data show the same fluence dependence as the collision-free data, except that the absolute yields are lower, due to the

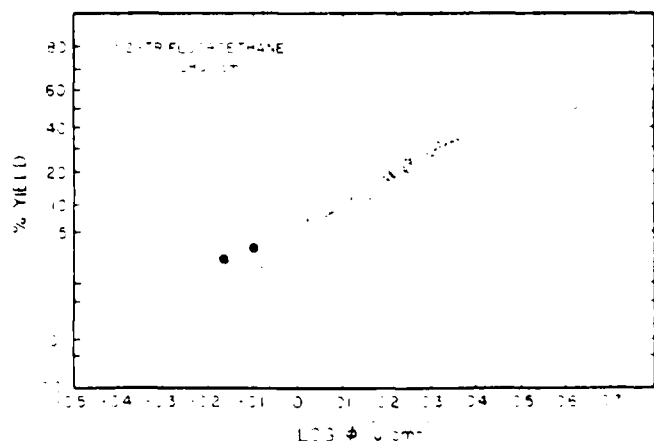


FIG. 1. Decomposition yields vs fluence at  $1079.85\text{ cm}^{-1}$ . Key:  $\circ$ —Lumonics laser;  $\diamond$ —Tachisto laser;  $\bullet$ —Tachisto laser, very large number of laser shots.

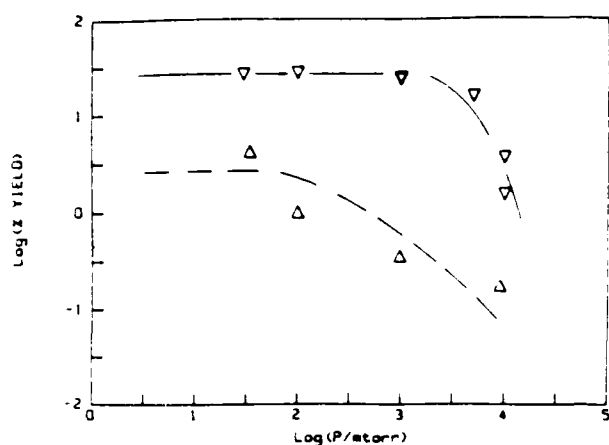


FIG. 2. Decomposition yield dependence on pressure, determined by the optoacoustic method. The curves are schematic. Upper curve:  $2.7 \text{ J cm}^{-2}$ ; absolute uncertainties are  $\pm 2\%$ . Lower curve:  $0.9 \text{ J cm}^{-2}$ ; absolute uncertainties are  $\pm 0.2\%$ .

higher pressures used and, perhaps, to small systematic errors in the fluence measurements.

The two series of optoacoustic measurements presented in Fig. 2 show the different effects of pressure on IRMPD yields at different laser fluences. At high fluence, the yield is not greatly affected, except at relatively high argon pressures. At low fluences, however, the yields are strongly affected by argon pressure over the entire range of pressure investigated.

#### Optoacoustic measurements of absorbed laser power

##### Calibration

The optoacoustic signals depend on gas composition, pressure, collisional energy transfer rates, laser energy, beam diameter, and spatial position of the microphone (see Ref. 5(d) for a fuller discussion), and careful calibration was necessary. Absolute calibration factors were obtained by using the absorption cross section as measured over a path length

of 30.5 cm and using the Tachisto laser and the Scientech power meter; Beer's Law fully described the experimental data. The absorption cross section measured in this way  $[(3.46 \pm 0.35) \times 10^{-9} \text{ cm}^2]$  is about a factor of 2 larger than that measured with a Digilab FTIR with  $0.1 \text{ cm}^{-1}$  resolution  $[(2.0 \pm 0.2) \times 10^{-19} \text{ cm}^2]$ . We concluded that the laser measurement is more pertinent to our experiments, considering the complex spectrum (Fig. 3) and possible coupling mechanisms that may be operative at high laser power.

At sufficiently low fluence, most molecules absorb no more than one photon and decomposition is not important. Extensive calibrations were carried out at low fluences by measuring the microphone signal for a fixed set of "hardware parameters" (e.g., fluence, laser beam diameter, and location of the microphone) and a fixed partial pressure of TFE diluted in various pressures of argon. The parameters were varied systematically to determine the saturation limit of the microphone and the effects of the parameters. For fixed laser beam spatial parameters and for TFE highly diluted in argon, the microphone signal was found to depend primarily on absorbed laser energy and slightly on argon pressure. The instrument response was directly proportional to absorbed laser power as long as the microphone was not overloaded. The calibration factors were found to depend linearly on  $\log(\text{pressure})$  for a wide range of experimental parameters, as shown in Fig. 4, where the calibration factor is given by<sup>5(d)</sup>

$$F = S_{OA} C_M / E_A \quad (2)$$

Here,  $S_{OA}$  is the microphone signal (arbitrary voltage units),  $C_M$  is the total heat capacity of the gas mixture at constant volume, and  $E_A$  is the absorbed energy per unit length. Based on Beer's law at the small absorbance limit and the measured cross section  $\sigma$ ,  $E_A$  is given by

$$E_A = E_L \sigma [\text{TFE}], \quad (3)$$

where  $E_L$  is the laser pulse energy and  $[\text{TFE}]$  is the TFE concentration in convenient units. For interpretation of the absorbed laser energy measurements, a least-squares fit to

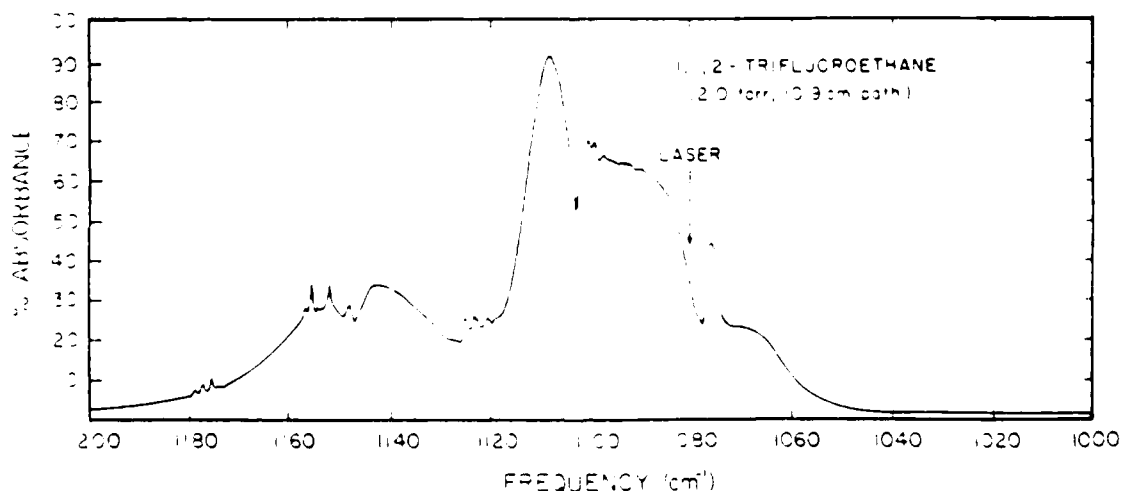


FIG. 3. Infrared spectrum of 1,1,2-trifluoroethane near  $1100 \text{ cm}^{-1}$  FTIR spectrum obtained with  $\approx 0.1 \text{ cm}^{-1}$  resolution; for vibrational assignment, see Ref. 8.

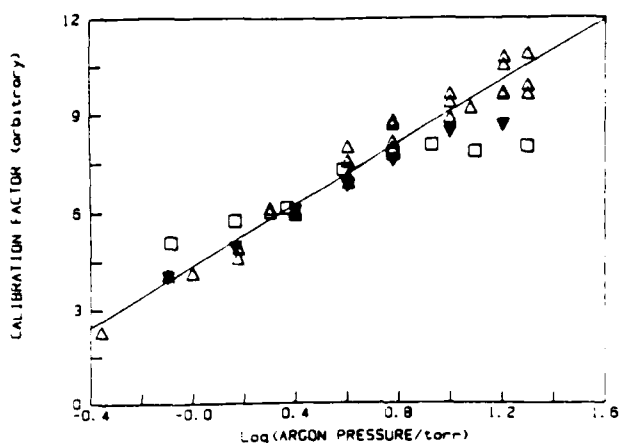


FIG. 4. Optoacoustic signal calibration curves. Pressures of TFE:  $\Delta$ —2.4 mTorr;  $\blacktriangledown$ —50 mTorr;  $\square$ —125 mTorr; solid line: least-squares fit to low-pressure points.

the experimental calibration data was used, as shown in the figure.

#### Absorbed laser energy measurements

Using the experimental calibration curve, we can determine the absorbed energy, based on the observed microphone signal and the gas composition. To place the absorbed energy on the molecular scale, it is conveniently expressed as the average number of absorbed photons per molecule, given by

$$\langle n \rangle = S_{OA} C_M / [F h \nu_0 [TFE]], \quad (4)$$

where  $h\nu_0$  is the laser photon energy and the other factors have been identified above. Using this expression places the absorbed energy on a reduced scale, enabling direct comparisons of absorbed energies obtained under widely different conditions.

Experiments were carried out to determine the effects of added argon and laser fluence on  $\langle n \rangle$ . Usually, better results were obtained in static experiments than in flowing gas systems, which suffered from fluctuations in total pressure and in gas composition. Care was taken to avoid depletion of the TFE in experiments with high laser fluence. The results are presented in Fig. 5, and they show no significant dependence on pressure for fluences up to about  $2 \text{ J cm}^{-2}$ . The results are highly consistent, with a relative uncertainty of about  $\pm 5\%$  and an absolute uncertainty estimated at about  $\pm 30\%$ , mostly due to the uncertainty in the fluence and energy measurements that went into calibration of the microphone.

At the highest fluences, decomposition of the TFE during the laser pulse may become significant, affecting the simple interpretation of the results. Although the reactions are slightly endothermic and can affect the optoacoustic signal to a small extent, the major uncertainty is due to the unknown extent of absorption of the laser photons by vibrationally hot reaction products. In the infrared fluorescence measurements on this system,<sup>7</sup> direct evidence was obtained for secondary photolysis of the products.

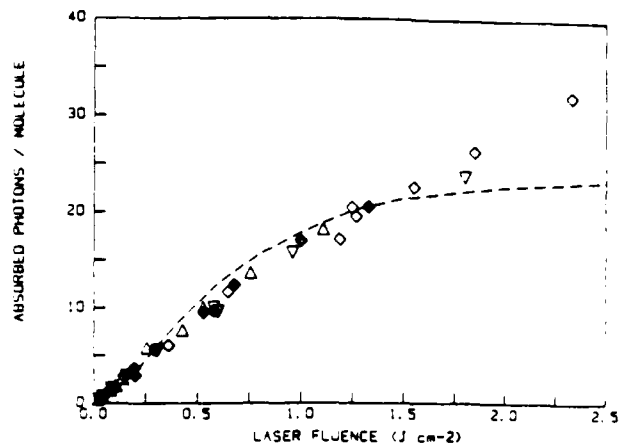


FIG. 5. Average number of photons absorbed per molecule vs fluence. Argon pressures:  $\blacktriangledown$ —0.5 Torr;  $\diamond$ —1.0 Torr;  $\Delta$ —20.0 Torr;  $\circ$ —10.0 Torr; dashed line: Master Equation calculation.

#### MASTER EQUATION MODEL

The basic Master Equation approach to simulating experiments such as these has been described in detail,<sup>6</sup> except for several significant improvements. Essentially, the approach<sup>15</sup> used Monte Carlo techniques to simulate random walks of individual molecules in energy space, subject to the properties of the molecule and its interactions with the laser photons.<sup>16</sup> Many such "trajectories" are calculated and the results are averaged, or otherwise stored for examination. Other than that used in calculating the vibrational densities of states, no intrinsic "graining" is imposed on the physics of the system, unlike approaches that use an "energy-grained" Master Equation. Thus, convergence of the solutions does not depend on grain size, although the precision obtainable depends on the number of trajectories calculated, as is usual in Monte Carlo simulations.<sup>16</sup>

The physical processes considered in the model include optical absorption and stimulated emission, collisional energy transfer, infrared fluorescence, and up to three unimolecular reaction channels; several models for some of these processes have been incorporated in the computer code as options.<sup>9</sup>

The Master Equation implementation has been significantly improved in several ways for present purposes. First, all densities of vibrational states are now calculated from exact counts of states,<sup>17</sup> rather than from the Whitten-Rabinovitch approximation<sup>18</sup> used earlier. For TFE, an energy grain of  $25 \text{ cm}^{-1}$  has proved to be adequate for the calculations. The densities of states for the first  $2500 \text{ cm}^{-1}$  of internal energy are stored in a 100-element array; in addition, the densities for the first  $50\,000 \text{ cm}^{-1}$  are stored in a second 100-element array. The density of states at any energy up to  $50\,000 \text{ cm}^{-1}$  is selected by interpolation between elements in one of these two arrays. Incorporation of exact state counts has made little difference in computed results, except for the distribution of initial energies selected. For example, now the thermal distribution is much more accurately produced, compared to the somewhat shifted version obtained<sup>6</sup> using the Whitten-Rabinovitch approximation.

The other improvements are concerned with the optical pumping and stimulated emission segments of the model. In addition to the former capability to consider a laser intensity that is constant for the entire duration of a trajectory and a laser pulse shape that decays exponentially, additional provision has been made for a laser pulse of constant duration and finite length. This capability enables investigation of post-pulse phenomena subsequent to a pulse of constant intensity. The second enhancement of the optical interaction model was to incorporate Quack's theory of infrared laser absorption/emission for his cases B and C.<sup>19</sup>

Prior to incorporation of Quack's theory in our model, we used a semiempirical expression for the absorption cross section dependence on vibrational energy.<sup>4,6,14,16</sup>

$$\sigma(E) = \sigma_0 [1 + E/h\nu_0]^{n(\lambda)}, \quad (5)$$

where  $\sigma_0$  is the absorption cross section for all molecules at the zero-point energy level,  $h\nu_0$  is the laser photon energy, and  $n(\lambda)$  is a parameter that depends on the wavelength of the laser. This expression has been used in Master Equation treatments of IRMPD with fair success, but recently, Haas and co-workers commented on the inadequacies of a Master Equation treatment that employed this type of expression.<sup>2</sup> In order to reduce the degree of empiricism somewhat, and because we also find Eq. (5) to be inadequate for treatment of the results obtained in the present work (see below), we implemented the Quack formalism for cases B and C.

Quack has described his statistical-dynamical theory extensively in the literature<sup>19</sup> and we will not attempt to repeat the details here. His approach is to evaluate the matrix elements for laser pumping and stimulated emission using a combination of *ab initio* theory and judicious approximations. The resulting expressions give the optical transition rates in terms of physically measurable quantities, with provision for empirical parametrization, where desirable.

According to Quack,<sup>19</sup> the optical transition rates for up-pumping from level  $M$  to  $M+1$  for both cases B and C are given by the expression

$$K_{M \rightarrow M+1}^B = 2\pi |V_{M+1,M}^0|^2 / \delta_{M+1}, \quad (6)$$

where  $\delta_{M+1}$  is the frequency spacing of effectively coupled states in the upper level and  $|V_{M+1,M}^0|$  is the absolute value of the matrix element connecting the two levels (each microcanonical level contains many individual quantum states). According to Quack,  $\delta_i$  can be related to the total density of vibrational states according to the expression

$$\delta_i = 2\pi c / \rho(E_i), \quad (7)$$

where  $c$  is the speed of light, and  $\rho(E_i)$  is the total density of vibrational states at the energy of level  $i$ . The matrix element is related to the laser intensity  $I$  and the integrated absorption cross section  $\int \sigma dx$ , by the expression

$$|V_{M+1,M}^0|^2 = \alpha \xi(E_M) \frac{\rho'(E_M) I \int \sigma dx}{\rho(E_{M+1}) \rho(E_M) \Delta E_Q h\nu_p}, \quad (8)$$

where  $\rho'(E)$  is the density of vibrational states with the pumped vibrational mode in the zero level,  $\Delta E_Q$  is the level width over which the matrix elements are approximately constant, and  $h\nu_p$  is the energy (expressed in  $\text{cm}^{-1}$ ) of the pumped mode. The factor  $\xi(E_M)$  allows empirical parame-

trization of the expression; when  $\xi(E_M) = 1.0$ , the parameters are assumed to be independent of internal energy and to equal those measured at low intensities. For intensities expressed in  $\text{W cm}^{-2}$ , state densities in states per  $\text{cm}^{-1}$ ,  $\sigma$  in  $\text{cm}^2$ ,  $\Delta E_Q$  in  $\text{cm}^{-1}$ , and  $dx$  in  $\text{cm}^{-1}$ , the proportionality constant is  $\alpha = 1.509 \times 10^{33}$ , to express the squared matrix element in units of  $\text{rad}^2 \text{s}^{-2}$ .

The down-pumping rates differ for cases B and C. For case B, the down-transition rate from level  $M$  to  $M-1$  is given by

$$K_{M-1,M}^B = K_{M-1,M} \frac{\rho(E_{M-1})}{\rho(E_M)}, \quad (9)$$

where the factors have been defined above. For case C, the down-transition rate is given by

$$K_{M-1,M}^C = K_{M-1,M}^B \frac{2\delta_M}{(\pi\sqrt{3}|V_{M,M-1}^0|^2)} \quad (10)$$

$$= \gamma K_{M-1,M}^B \left[ \frac{\rho(E_{M-1}) \Delta E_Q h\nu_p}{\rho(E_M) \rho'(E_{M-1}) \int \sigma dx} \right]^{1/2}, \quad (11)$$

where the symbols have the same meanings and units as above, and the proportionality constant  $\gamma$  is  $1.784 \times 10^{-6}$  for the transition rate expressed in  $\text{s}^{-1}$ . The crossover from case C to case B at low energy and/or low intensity is treated by selecting the larger of the two calculated transition rates, as described by Quack.

For 1,1,2-trifluoroethane, the molecular parameters needed for use of the Quack expressions are known and are summarized in Tables I and II. The expressions can be empirically adjusted<sup>19</sup> by treating  $\Delta E_Q$  as a parameter used in concert with  $\xi(E)$ , as discussed below. Densities of vibrational states were obtained from exact counts by using the vibrational assignment for the molecule and assuming harmonic oscillators. For the density of states calculations, the internal rotor was treated as a  $117 \text{ cm}^{-1}$  vibration.

## DISCUSSION

The two experimental techniques employed in this investigation provide information about the IRMPA process over two complementary internal energy ranges. The optoacoustic measurements are most accurate for low fluences, or when reaction is not important. On the other hand, the IRMPD measurements require that molecules be pumped above the reaction threshold, and it has been shown that the technique provides information mostly about the reaction threshold region and above.<sup>4,14,16</sup>

The absorbed energy measurements show little dependence on pressure, and thus we conclude that at low pressures, where collisional deactivation during the pumping process is unimportant, the measurements reflect the average energy of the nascent population. Since the reaction threshold energies are about  $24\,000 \text{ cm}^{-1}$ , the optoacoustic measurements can be interpreted in a straightforward way up to  $\langle n \rangle \approx 22$ . Above that value, the extent of decomposition will affect the results in three ways: (1) depletion of the parent molecules during the laser pulse will mean fewer photons absorbed, (2) the reaction thermochemistry can affect

TABLE I. Molecular properties of 1,1,2-trifluoroethane.

Property	Value	Reference	
Vibrational frequency assignment			
Heat capacity ( $C_p$ )	$16.29 + 0.033(T - 300)$ Gibbs mol <sup>-1</sup>	a	
Lennard-Jones $\sigma$	5.28 Å	c	
Lennard-Jones $\epsilon/k$	325 K		
$h\nu_p$ (pumped mode: $\nu_{11}$ )	1076 cm <sup>-1</sup>		
$\int \sigma dx$	$(5 \pm 1) \times 10^{-18}$ cm	d	
Unimolecular reaction parameters (Whitten-Rabinovitch)			
	Reaction: A B C		
$(h\nu)_{TST}$	941.62	917.37	906.77
$E_{crit}$	23 714	23 714	24 413
TST Zero point energy	9 751.0	9 538.5	9 641.0
Whitten-Rabinovitch $\beta$	1.353	1.377	1.379
$\sigma_{path} \times (I = 1)$	0.65	2.50	2.02

<sup>a</sup> V. F. Kalasinsky, H. V. Anjaria, and T. S. Little, *J. Phys. Chem.* **86**, 1351 (1982).

<sup>b</sup> Calculated from the vibrational assignment.

<sup>c</sup> Estimated using Lyderson's method as described in R. C. Reid and T. K. Sherwood, *The Properties of Gases and Liquids*, 2nd ed. (McGraw-Hill, New York, 1966).

<sup>d</sup> Measured in this work; see FTIR spectrum in Fig. 3.

<sup>e</sup> Whitten-Rabinovitch parameters for the transition states were derived from the detailed transition state frequencies given by B. E. Holmes, D. W. Setser, and G. O. Pritchard, *Int. J. Chem. Kinet.* **8**, 215 (1976); RRKM  $k(E)$ 's were calculated using the TFE state densities and Whitten-Rabinovitch approximation for the sums of states.

the heat release, and (3) the [hot] reaction products produced during the pulse, or in previous pulses, may absorb the laser light. Inspection of Fig. 5 shows that with 10 Torr argon added,  $\langle n \rangle > 32$ , much higher than the reaction threshold energy. At this high pressure, decomposition is inhibited by collisional deactivation of excited molecules and the reactant is not depleted. Indeed, the collisional deactivation rate is fast enough so that the excited molecules are never pumped very high on the energy ladder.

The absence of a pressure dependence at relatively high pressures, where collisional deactivation during the laser pulse is important, indicates that the net optical absorption rate of the excited molecules does not depend strongly on internal energy. Inspection of the 10 Torr added argon data set in Fig. 5 shows that it is virtually indistinguishable from data sets obtained at much lower pressures. More quantitative conclusions about the optical pumping process require the numerical calculations described below.

The IRMPD measurements probe molecules pumped above the reaction threshold. When the yields are low, the decomposing molecules represent only the high energy "tail" of the population distribution, which is highly sensitive to several effects, including the optical pumping process and collisional energy transfer. At sufficiently low pressures, homogeneous collisional effects are unimportant, and the IRMPD yields reflect the fraction of molecules pumped above the reaction threshold that react before deactivation at

the walls of the cell. Since drift times to the cell walls are of the order of  $3 \times 10^{-4}$  s, the decomposition yield at low pressure equals the fraction of molecules that attain energies high enough to have specific unimolecular rate constants  $k(E) > 3 \times 10^3$  s<sup>-1</sup> (i.e.,  $E > 26\,000$  cm<sup>-1</sup>).

Information about the optical pumping process can be obtained from the dependence of the collision-free IRMPD yield on fluence. As a class, systems with optical pumping properties that can be described by the simple power-law equation (5) have decomposition yields that can be plotted linearly vs log(fluence) on probability graph paper, as has been discussed elsewhere.<sup>14,16</sup> The VLPΦ experimental data are presented on such a log-normal plot in Fig. 1 and the resulting line is clearly curved, indicating that the optical pumping is not well described by Eq. (5). The heuristic approach taken in our earlier work in order to account for such curvature was to assume that the excited molecules were partitioned into two or more population subsets with different optical pumping parameters.<sup>20</sup> This approach could have been taken in the present work, but Quack's more sophisticated theory<sup>19</sup> accounts satisfactorily for the experimental observations without recourse to the multiple-population model.

A more complete discussion of collisional energy transfer in this system will appear elsewhere,<sup>21</sup> but IRMPD yield data obtained with the optoacoustic technique are presented in Fig. 2. These results show that, as expected, the low fluence data are far more susceptible to collisional effects than data obtained at higher fluences. The high energy tail of the excited molecule distribution is sensitively affected by collisions, even at pressures as low as 35 mTorr. (Note that our experimental tests showed that the VLPΦ data obtained at 20 mTorr were not significantly affected by total pressure.) The decreased yield is due almost entirely to "post-pulse" collisional deactivation of excited molecules that have energies only a little above the reaction threshold. In

TABLE II. Quack theory fitted parameters.

Parameter	Value
Pulse width	$125 \pm 15$ ns
$\Delta E_0$	$4 \pm 1$ cm <sup>-1</sup>
$W$	$23\,700 \pm 100$ cm <sup>-1</sup>
$m$	$20 \pm 5$

addition, mass transport to the cell wall is affected by the higher pressures, and the detailed differences in the collision efficiency of walls vs gas phase must be taken into account for a full description.<sup>22</sup> Such a description is feasible, but it is beyond the scope of the present work.

To obtain more quantitative information about the pumping process, the Master Equation approach described above was utilized and the effects of many parameters were investigated. Insofar as possible, experimentally measured parameters were used in order to limit the latitude of the calculations. Many combinations of assumptions and input parameters were investigated to determine whether they were consistent with the experimental data, but it was found that the two sets of experimental data combined with knowledge of TFE molecular properties constrained the latitude of the calculations greatly, and a satisfactory simulation of the experiments was difficult to achieve.

The *unsatisfactory* attempts at simulation of the experiments included the following combinations of assumptions:

(1) Exponential or square laser pulse used with the power-law absorption cross section in Eq. (5): This combination could be made to fit the absorbed energy measurements very well by using the measured cross section and adjusting the parameter  $n(\lambda)$ , but the predicted yield vs fluence results were too steep on a log-normal plot, as shown in our preliminary report.<sup>23</sup> Also, the simulated log-normal plot was a straight line, unlike the experimental data.

(2) Exponential laser pulse and Quack's theory with  $\xi(E) = 1.0$ : Here, the absorbed energy measurements could be well simulated by varying the parameter  $\Delta E_0$ , but the predicted reaction yields were much too high. Furthermore, the pulse decay time significantly affected the predicted value of  $\langle n \rangle$  at a given fluence. This is because the transition between cases B and C depends on laser intensity, and the down-pumping rate in case C is much greater than in case B. Molecules pumped up, early in the pulse under case B conditions, could be rapidly down pumped later in the pulse, when the intensity is lower and case C is operative. This effect may be observable in carefully designed experiments; its presence may indicate that an accurate simulation of the laser pulse is necessary for more detailed calculations.

(3) Square laser pulse and Quack's theory with  $\xi(E) = 1.0$ : To simplify the model, a square pulse was assumed. This simplified version gave good agreement with  $\langle n \rangle$  for suitable choices of  $\Delta E_0$  and the pulse width, but the predicted reaction yields were much too high, indicating that the average molecules could be well modeled, but the high-energy tail of the distribution (that resulted in decomposition) was predicted to be too highly populated.

Since the Quack theory with  $\xi(E) = 1.0$  (and appropriate choices of  $\Delta E_0$  and laser pulse width) fitted the experimental data on absorbed laser energy very well, our approach was to choose a functional form that gave  $\xi(E) = 1.0$  at low internal energies, but allowed simple variations at higher energies. A first attempt at a functional form for  $\xi(E)$  incorporated a Lorentzian with "width" and "center" that could vary linearly as a function of internal energy, as suggested by Quack.<sup>19(d)</sup> This approach was not successful, although nonlinear dependencies on internal energy could

probably be made to work. Inspection of the infrared spectrum of TFE (Fig. 3) shows that at least two fundamental transitions are important, and a simple Lorentzian is not adequate.

The second attempt at choosing a functional form for  $\xi(E)$  was successful. The assumed form incorporates only two empirical parameters and it gives  $\xi(E) = 1.0$  at low energies:

$$\xi(E) = \exp\{- (E/W)^m\}. \quad (12)$$

Although this function is arbitrary and not unique, it provides a smooth transition between the optical properties of the molecule at low energies, where they can be measured with a spectrometer, and at high energies, where the anharmonicities may become very significant.

By a process of trial and error, a combination of parameters (Table II) was found that gives model simulations in good agreement with the experimental data sets, as shown in Figs. 1 and 5. The calculated yield vs fluence results are in excellent agreement with the experimental data over virtually the entire fluence range investigated. The minor discrepancy at very low fluence may be due to experimental artifacts and/or to inadequacies of the model for the extremely small populations at the highest part of the distribution. The calcu-

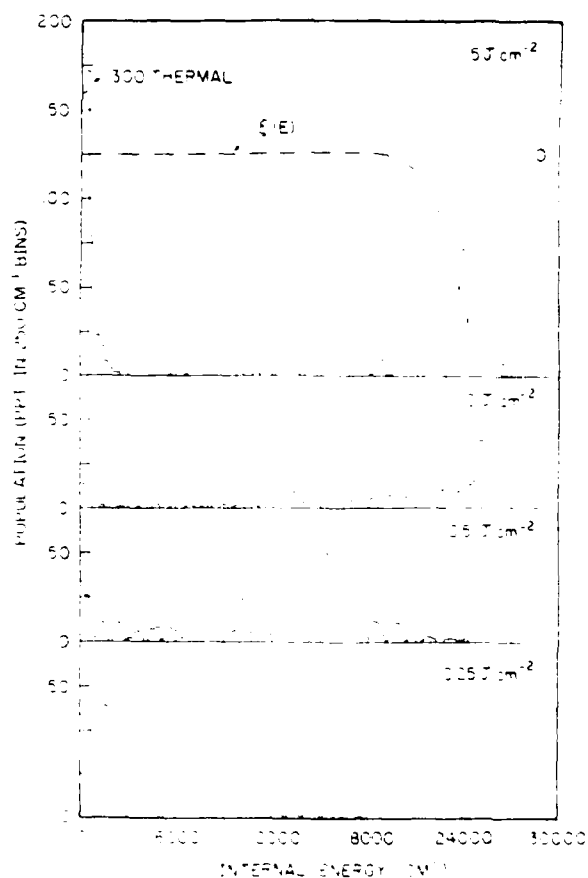


FIG. 6. Population distributions. Each panel corresponds to a different laser fluence. For reference, the 300 K thermal distribution and the function  $\xi(E)$  are shown in the top panel (the population distribution for  $1.5 \text{ J cm}^{-2}$  is essentially zero below  $5000 \text{ cm}^{-1}$ ).

TABLE I. Molecular properties of 1,1,2-trifluoroethane.

Property	Value	Reference	
Vibrational frequency assignment			
Heat capacity ( $C_v$ )	$16.29 + 0.033(T - 300)$ Gibbs mol <sup>-1</sup>	a	
Lennard-Jones $\sigma$	5.28 Å	c	
Lennard-Jones $\epsilon/k$	325 K		
$h\nu_p$ (pumped mode: $\nu_{11}$ )	1076 cm <sup>-1</sup>		
$\sigma dx$	$(5 \pm 1) \times 10^{-18}$ cm	d	
Unimolecular reaction parameters (Whitten-Rabinovitch)			
	Reaction: A B C	e	
$\langle h\nu \rangle_{TST}$	941.62	917.37	906.77
$E_{int}$	23 714	23 714	24 413
TST Zero point energy	9 751.0	9 538.5	9 641.0
Whitten-Rabinovitch $\beta$	1.353	1.377	1.379
$\sigma_{path} \times (I^\ddagger / I)$	0.65	2.50	2.02

<sup>a</sup> V. F. Kalasinsky, H. V. Anjaria, and T. S. Little, *J. Phys. Chem.* **86**, 1351 (1982).

<sup>b</sup> Calculated from the vibrational assignment.

<sup>c</sup> Estimated using Lyderson's method as described in R. C. Reid and T. K. Sherwood, *The Properties of Gases and Liquids*, 2nd ed. (McGraw-Hill, New York, 1966).

<sup>d</sup> Measured in this work; see FTIR spectrum in Fig. 3.

<sup>e</sup> Whitten-Rabinovitch parameters for the transition states were derived from the detailed transition state frequencies given by B. E. Holmes, D. W. Setser, and G. O. Pritchard, *Int. J. Chem. Kinet.* **8**, 215 (1976); RRKM  $k(E)^\ddagger$ 's were calculated using the TFE state densities and Whitten-Rabinovitch approximation for the sums of states.

the heat release, and (3) the [hot] reaction products produced during the pulse, or in previous pulses, may absorb the laser light. Inspection of Fig. 5 shows that with 10 Torr argon added,  $\langle n \rangle > 32$ , much higher than the reaction threshold energy. At this high pressure, decomposition is inhibited by collisional deactivation of excited molecules and the reactant is not depleted. Indeed, the collisional deactivation rate is fast enough so that the excited molecules are never pumped very high on the energy ladder.

The absence of a pressure dependence at relatively high pressures, where collisional deactivation during the laser pulse is important, indicates that the net optical absorption rate of the excited molecules does not depend strongly on internal energy. Inspection of the 10 Torr added argon data set in Fig. 5 shows that it is virtually indistinguishable from data sets obtained at much lower pressures. More quantitative conclusions about the optical pumping process require the numerical calculations described below.

The IRMPD measurements probe molecules pumped above the reaction threshold. When the yields are low, the decomposing molecules represent only the high energy "tail" of the population distribution, which is highly sensitive to several effects, including the optical pumping process and collisional energy transfer. At sufficiently low pressures, homogeneous collisional effects are unimportant, and the IRMPD yields reflect the fraction of molecules pumped above the reaction threshold that react before deactivation at

the walls of the cell. Since drift times to the cell walls are of the order of  $3 \times 10^{-4}$  s, the decomposition yield at low pressure equals the fraction of molecules that attain energies high enough to have specific unimolecular rate constants  $k(E) > 3 \times 10^3$  s<sup>-1</sup> (i.e.,  $E > 26\,000$  cm<sup>-1</sup>).

Information about the optical pumping process can be obtained from the dependence of the collision-free IRMPD yield on fluence. As a class, systems with optical pumping properties that can be described by the simple power-law equation (5) have decomposition yields that can be plotted linearly vs log(fluence) on probability graph paper, as has been discussed elsewhere.<sup>14,16</sup> The VLPΦ experimental data are presented on such a log-normal plot in Fig. 1 and the resulting line is clearly curved, indicating that the optical pumping is not well described by Eq. (5). The heuristic approach taken in our earlier work in order to account for such curvature was to assume that the excited molecules were partitioned into two or more population subsets with different optical pumping parameters.<sup>20</sup> This approach could have been taken in the present work, but Quack's more sophisticated theory<sup>19</sup> accounts satisfactorily for the experimental observations without recourse to the multiple-population model.

A more complete discussion of collisional energy transfer in this system will appear elsewhere,<sup>21</sup> but IRMPD yield data obtained with the optoacoustic technique are presented in Fig. 2. These results show that, as expected, the low fluence data are far more susceptible to collisional effects than data obtained at higher fluences. The high energy tail of the excited molecule distribution is sensitively affected by collisions, even at pressures as low as 35 mTorr. (Note that our experimental tests showed that the VLPΦ data obtained at 20 mTorr were not significantly affected by total pressure.) The decreased yield is due almost entirely to "post-pulse" collisional deactivation of excited molecules that have energies only a little above the reaction threshold. In

TABLE II. Quack theory fitted parameters.

Parameter	Value
Pulse width	$125 \pm 15$ ns
$\Delta E_Q$	$4 \pm 1$ cm <sup>-1</sup>
$W$	$23\,700 \pm 100$ cm <sup>-1</sup>
$m$	$20 \pm 5$

lated curve for  $\langle n \rangle$  vs fluence in Fig. 5 corresponds to an assumed argon pressure of 1.0 Torr, and the saturation effect due to the function  $\xi(E)$  is clearly seen; at higher pressures, molecules are deactivated before reaching such high energies, and the predicted behavior then resembles that observed in the experiments with 10 Torr argon.

The fitted parameters appear to be reasonable, but they are not unique, because they depend on the assumed functional form for  $\xi(E)$ . Within the framework of our assumptions, however, there is very little latitude for variation of the parameters, as indicated by the estimated uncertainties.

Comparison of the parameters in Table II with the known molecular properties of TFE and the experimental conditions shows good agreement. For example, the laser pulse width of  $125 \pm 15$  ns for a simulated square pulse is roughly similar to the typical  $\text{CO}_2$  TEA laser pulse, which is comprised of many irregularly modulated spikes enclosed by an average amplitude envelope consisting of a 100 ns pulse with a 1–2  $\mu\text{s}$  tail. Also, the parameter  $\Delta E_Q$  is expected to be of the same order as the width of the infrared absorption band<sup>19</sup>; in TFE, the laser photons are  $4 \text{ cm}^{-1}$  out of resonance with the  $\nu_{11}$  Q branch (for the  $C_1$  conformer, the predominant form in the gas phase) at  $1076 \text{ cm}^{-1}$ , which is about  $2.5 \text{ cm}^{-1}$  in width, compared to  $\Delta E_Q = 4 \pm 1 \text{ cm}^{-1}$ . Most interesting, however, is the fitted value of the parameter  $W$ .

In Eq. (12), the parameter  $W$  is the energy at which  $\xi(E) = 1/e$  and the optical coupling matrix element is much reduced compared to its value for transitions at low internal energies. There can be several reasons for a reduction in magnitude of the matrix elements, but a good explanation is provided if the transition energies shift away from resonance due to anharmonicity. The value of  $W$  depends slightly on that of the parameter  $m$ , but for  $m = 20$ , the uncertainty in  $W$  is quite small.

The fact that the value of  $W$  is so close to the reaction thresholds is highly suggestive that anharmonicity introduced by the open reaction channels plays an important role in the spectroscopic properties of this highly vibrationally excited molecule. Although  $\xi(E)$  is not a unique function, its general behavior may provide a good semiquantitative description of the optical matrix elements near the reaction thresholds. Based upon our experience in attempting to simulate the experimental data presented here, we conclude that, within the framework of the Quack theory, the matrix elements must undergo a drastic change near the reaction thresholds. If our conclusion is correct, this may be the first time the effect has been observed in highly vibrationally excited polyatomic molecules.

The reactions in TFE are HF eliminations that must pass through molecular configurations starting from single-bonded carbon atoms with  $sp^3$  hybridization, through intermediate configurations (i.e., a transition state), to doubly bonded carbon atoms with  $sp^2$  hybridization. The  $\nu_{11}$  infrared transition at  $1076 \text{ cm}^{-1}$  is an asymmetric C–F stretching mode, a mode that must be affected by a change in hybridization of the carbon atom: as the hybridization changes from  $sp^3$  to  $sp^2$ , the C–F bond will be slightly strengthened, resulting in changes in vibrational frequen-

cies. Specifically, the  $1076 \text{ cm}^{-1}$  C–F stretch mode frequency in TFE may be compared to the C–F stretch modes in *cis*- and *trans*-1,2-difluoroethylene (product molecules), which have frequencies of 1014, 1127, 1123, and  $1159 \text{ cm}^{-1}$ , far out of resonance with the laser photons. Since every C–F bond in TFE (even those not directly involved in the HF elimination) undergoes a change in hybridization when reaction occurs, it is not surprising that the transition matrix elements for the C–F stretch modes drastically decrease in magnitude at energies close to the reaction thresholds.

The primary objective of this work was to determine the population distributions produced in TFE by IRMPA. Although not unique, the model results probably represent a very good approximation to the distribution functions, especially considering the narrow latitudes available for satisfactory simulation of the two data sets. The population distributions predicted for several laser fluences are presented in Fig. 6 along with a plot of  $\xi(E)$ . Note that the  $250 \text{ cm}^{-1}$  "binning" of the calculated results was for bookkeeping purposes and had no effect on the actual calculation.

The calculated distributions predict that at low and intermediate fluences, a significant fraction of molecules remains in the initial thermal distribution, but that fraction becomes much smaller at higher fluences. At all fluences, the initial thermal distribution is translated upwards by integral numbers of photon energies, resulting in a series of peaks that have about the same width as the initial thermal distribution. Also, the overall dispersion of energies is quite large, compared to the mean. At high fluences, however, the dispersion becomes much smaller, as molecules "stack up" at high energies, due to the fall off of  $\xi(E)$ . On a longer time scale, most molecules will decompose, because they have energies greater than the reaction thresholds.

These population distributions illustrate that IRMPA is effective in exciting most molecules in the laser beam and that the distributions are quite broad. For effective use of the technique in laboratory studies of other molecules, efforts are necessary to elucidate the distribution functions produced. Absorbed energy measurements taken alone are not sufficient to determine the population distributions, since any of the combinations of assumptions described above could simulate the optoacoustic experiments.

The combinations of experimental measurements that are most effective in constraining the computer simulations are those that measure different attributes of the population distributions. For example, in the present study, the absorbed energy measurements gave information mostly about the mean energy (the first moment of the population distribution), while the decomposition yield vs fluence measurements probed the high energy tail of the distribution function. In Fig. 7,  $\langle E \rangle$  is plotted as a function of  $\langle n \rangle$  to illustrate the direct connection between the first moment of the population distribution and the experimental observable. Thus, the experimental approach can be based on measuring properties that depend on the individual moments of the distribution function sought.

Some experimental measures that have not been considered here are the chemical reaction branching ratios to form the isomeric ethylene products. Branching ratio measure-

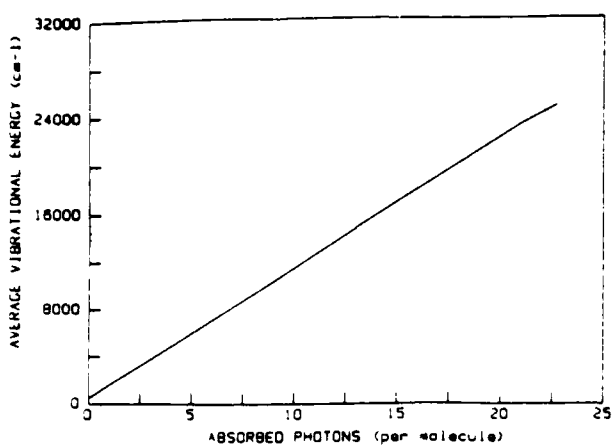


FIG. 7. Calculated values for  $\langle E \rangle$  as a function of  $\langle n \rangle$ . Note that the average thermal vibrational energy of TFE at 300 K is about  $470 \text{ cm}^{-1}$ .

ments are quite feasible in many systems and, in many cases, can give useful information. In this system, however, the reaction threshold energies are so close together that the relative yields are insensitive to small variations of the parameters in Table II. For example, variation of the parameter "m" from  $m = 15$  to  $m = 25$  is calculated to change the relative yield of 1,1-difluoroethylene from  $\approx 0.14$  to  $\approx 0.16$ . This variation is too small to be useful in refining the parameter values in the present investigation.

In the present study, the strategy of using a combination of experimental techniques to measure different attributes has resulted in information about the population distributions formed by IRMPA. This information will be used in subsequent studies of collisional energy transfer<sup>21</sup> and bimolecular reactions. In the following paper,<sup>22</sup> the calculated population distributions are used to predict infrared emission intensities, which are then compared to those observed in experiments.

## ACKNOWLEDGMENTS

The authors gratefully acknowledge financial support from the U.S. Army Research Office. JMZ acknowledges a fellowship from the Swiss Fonds National, and TCB thanks K. D. King at the University of Adelaide for his support and encouragement. Many of the numerical calculations were carried out in the Chemical Physics Laboratory at SRI using the VAX computing facility, which was provided by a grant from the National Science Foundation. The authors are happy to acknowledge the helpful conversations with D. W.

Setser, who also provided useful technical information on several molecules studied in his laboratory.

<sup>1</sup>For recent reviews, see (a) N. Bloembergen and E. Yablonovitch, *Phys. Today* **31**, 32 (1978); (b) P. A. Schultz, A. S. Sudbo, D. J. Krajnovich, H. S. Kwok, Y. R. Shen, and Y. T. Lee, *Annu. Rev. Phys. Chem.* **30**, 379 (1979); (c) M. F. Goodman, J. Stone, and E. Thiele, in *Multiple-Photon Excitation and Dissociation of Polyatomic Molecules*, edited by C. D. Cantrell (Springer, Berlin, 1980); (d) J. L. Lyman, G. P. Quigley, and O. P. Judd *ibid.*; (e) D. S. King, *Dynamics of the Excited State*, edited by K. P. Lawley (Wiley, New York, 1982), p. 105.

<sup>2</sup>S. Ruhman, O. Anner, and Y. Haas, *J. Phys. Chem.* **88**, 6397 (1984).

<sup>3</sup>For example, see J. W. Hudgens and J. D. McDonald, *J. Chem. Phys.* **76**, 173 (1982).

<sup>4</sup>(a) D. M. Golden, M. J. Rossi, A. C. Baldwin, and J. R. Barker, *Acc. Chem. Res.* **14**, 56 (1981); (b) M. J. Rossi, J. R. Barker, and D. M. Golden, *J. Chem. Phys.* **76**, 406 (1982).

<sup>5</sup>(a) R. D. Bates, Jr., G. W. Flynn, and J. K. Knudson, *J. Chem. Phys.* **53**, 3621 (1970); (b) *Opto-Acoustic Spectroscopy and Detection*, edited by Y. H. Pao (Academic, New York, 1977); (c) N. Presser, J. R. Barker, and R. J. Gordon, *J. Chem. Phys.* **78**, 2163 (1983); (d) J. R. Barker, L. Brouwer, R. Patrick, M. Rossi, P. L. Trevor, and D. M. Golden, *Int. J. Chem. Kinet.* (in press).

<sup>6</sup>(a) J. R. Barker, *Chem. Phys.* **77**, 301 (1983); (b) J. R. Barker and R. E. Golden, *J. Phys. Chem.* **88**, 1012 (1984).

<sup>7</sup>J.-M. Zellweger, T. C. Brown, and J. R. Barker, *J. Chem. Phys.* **83**, 6261 (1985).

<sup>8</sup>V. F. Kalasinsky, H. Anjaria, and T. S. Little, *J. Phys. Chem.* **86**, 1351 (1982).

<sup>9</sup>B. E. Holmes, D. W. Setser, and G. O. Pritchard, *Int. J. Chem. Kinet.* **8**, 215 (1976), and references therein.

<sup>10</sup>D. M. Golden, G. N. Spokes, and S. W. Benson, *Angew. Chem., Int. Ed. Engl.* **12**, 534 (1973).

<sup>11</sup>J. S. Chang, J. R. Barker, J. E. Davenport, and D. M. Golden, *Chem. Phys. Lett.* **60**, 385 (1979).

<sup>12</sup>For a discussion of intensity profiles and deconvolution considerations, see A. C. Baldwin and J. R. Barker, *J. Chem. Phys.* **74**, 3823 (1981).

<sup>13</sup>(a) T. Shimanouchi, *Tables of Molecular Vibrational Frequencies*, Natl. Stand. Ref. Data Serv. Natl. Bur. Stand. **39** (U.S. GPO, Washington, D.C., 1972), Vol. 1, 39, (1972); (b) T. Shimanouchi, *J. Phys. Chem. Ref. Data* **6**, 993 (1977).

<sup>14</sup>A. C. Baldwin and J. R. Barker, *J. Chem. Phys.* **74**, 3813 (1981).

<sup>15</sup>D. T. Gillespie, *J. Comput. Phys.* **22**, 403 (1976); *J. Phys.* **81**, 2340 (1977); *J. Comput. Phys.* **28**, 395 (1978).

<sup>16</sup>J. R. Barker, *J. Chem. Phys.* **72**, 3686 (1980).

<sup>17</sup>S. E. Stein and B. S. Rabinovitch, *J. Chem. Phys.* **58**, 2438 (1973).

<sup>18</sup>G. Z. Whitten and B. S. Rabinovitch, *J. Chem. Phys.* **38**, 2466 (1963); **41**, 1883 (1964).

<sup>19</sup>(a) M. Quack, *J. Chem. Phys.* **69**, 1282 (1978); (b) *Chem. Phys. Lett.* **65**, 140 (1979); (c) Ber. Bunsenges. *Phys. Chem.* **83**, 757 (1979); (d) **85**, 318 (1981); *Dynamics of the Excited State*, edited by K. P. Lawley (Wiley, New York, 1982), 395.

<sup>20</sup>A. C. Baldwin and J. R. Barker, *J. Chem. Phys.* **74**, 3823 (1981).

<sup>21</sup>J.-M. Zellweger, T. C. Brown, and J. R. Barker, *J. Phys. Chem.* (to be published).

<sup>22</sup>For detailed treatments of heterogeneous deactivation and mass transport to the cell walls in other systems, see (a) R. G. Gilbert, T. T. Nguyen, and K. D. King, *Int. J. Chem. Kinet.* **11**, 317 (1979); (b) R. G. Gilbert and K. D. King, *Chem. Phys.* **49**, 367 (1980).

<sup>23</sup>T. C. Brown, K. D. King, J.-M. Zellweger, and J. R. Barker, *Ber. Bunsenges. Phys. Chem.* **89**, 301 (1985).

TABLE I: Frequencies and Anharmonicities (in  $\text{cm}^{-1}$ )

A. Water <sup>11</sup>					
Frequencies ( $\omega_i$ )					
3656.65	1594.59	3755.79			
Anharmonicity Matrix ( $X_{ij}$ )					
-42.576	-15.933	-165.824			
-15.933	-16.813	-20.332			
-165.824	-20.332	-47.566			
B. Formaldehyde <sup>12</sup>					
Frequencies ( $\omega_i$ )					
2811.42	1755.858	1500.32	1170.224	2861.30	1250.565
Anharmonicity Matrix ( $X_{ij}$ )					
-28.95	1.15	-23.03	-10.099	-193.32	-49.78
1.15	-9.926	-8.26	-7.199	-17.23	6.581
-23.03	-8.26	-1.64	-1.769	6.00	-29.861
-10.099	-7.199	-1.769	-3.157	-13.35	-2.86
-193.32	-17.23	6.00	-13.35	-17.97	-17.63
-49.78	6.581	-29.861	-2.86	-17.63	-1.567

These expressions define the integration region boundary, and therefore the sampling domain completely encloses the integration region when  $\beta > 1$ . When  $\beta = 1$ , the sampling domain and the integration region are identical, producing 100% sampling efficiency.

For degrees of freedom other than vibrations, a sampling boundary that closely resembles the integration region boundary may be chosen for ease of calculation. It is not always desirable to include high-order effects in the sampling boundaries, because of the computational labor involved. When carrying out the sampling, we will include the higher order effects in calculating  $f(g)$  (see eq 7). In this way, couplings among vibrations, vibrations/rotations, Coriolis coupling, Fermi interactions, etc., are incorporated in the Monte Carlo integration.

## Results and Discussion

**Monte Carlo Integration.** The Monte Carlo sampling algorithm and sampling domain described above were tested for accuracy by comparisons with exact counts of states based on spectroscopic vibrational constants for water and formaldehyde presented in Table I. Although the spectroscopic data were obtained for energies only up to about 10 000  $\text{cm}^{-1}$  and they may not be appropriate for higher energies, we have used them at energies up to 40 000  $\text{cm}^{-1}$  solely for the purpose of testing the Monte Carlo technique. The exact counts were performed by using the Stein-Rabinovitch method with a grain size of 2.7  $\text{cm}^{-1}$ .

The harmonic oscillator calculations were performed by using the tabulated frequencies but setting all of the anharmonicities equal to zero; the tests using anharmonic separable oscillators were carried out by keeping the diagonal anharmonicities but neglecting the off-diagonal anharmonicities. We chose not to employ more accurate local mode descriptions of the C-H stretching vibrations,<sup>18</sup> because such descriptions require additional calculations and knowledge of the off-diagonal couplings between the stretching modes and they neglect the other off-diagonal couplings.

In Figure 2, the test results are presented as ratios of the Monte Carlo results divided by the exact-count results. The error bars were calculated according to eq 8, and they represent  $\pm 1\sigma$ . In all four of the test cases, the ratio of Monte Carlo/exact is equal to unity within  $1\sigma$  for most of the data points. Fewer than one-third of the test points ( $E > 0$ ) deviate more than  $\pm 1\sigma$  from unity, as expected on the basis of the normal error distribution. In other tests (not shown), the results were equally satisfactory, and it was found, as expected, that the standard deviation is inversely proportional to the square root of the number of trials.

Tests were also performed to determine whether the sampling domain completely enclosed the integration volume and whether the achievable precision was satisfactory. The sampling boundary was defined as described above, and the parameter  $\beta$  was varied

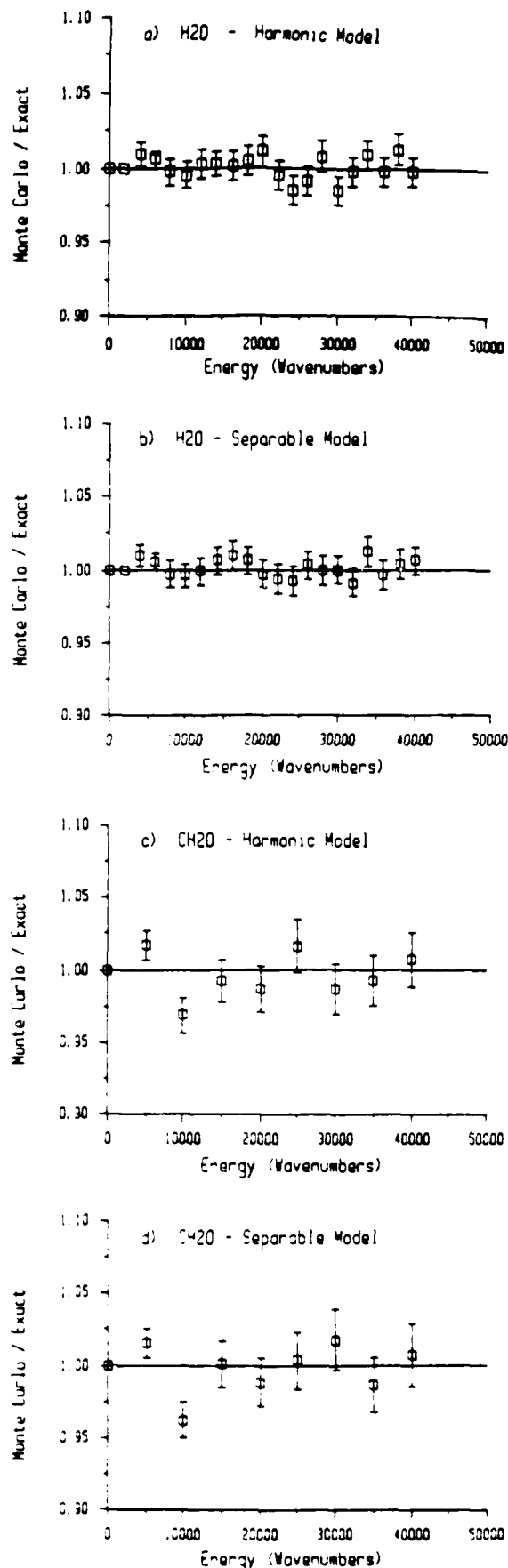


Figure 2. Accuracy tests. (a) water, harmonic oscillator model; (b) water, separable anharmonic oscillator model; (c) formaldehyde, harmonic oscillator model; (d) formaldehyde, separable anharmonic oscillator model.

TABLE II: Dependence on  $\beta$  and Number of Trials

energy	$\beta$	sum	trials	efficiency, %
Water (Coupled)				
40 000	1.00	$(1.215 \pm 0.006) \times 10^3$	50 000	100
40 000	1.01	$(1.234 \pm 0.012) \times 10^3$	17 532	91
40 000	1.25	$(1.226 \pm 0.019) \times 10^3$	25 000	19
Formaldehyde (Coupled)				
10 000	1.01	$(6.320 \pm 0.075) \times 10^2$	100 000	92
20 000	1.01	$(1.573 \pm 0.025) \times 10^4$	100 000	86
30 000	1.01	$(1.392 \pm 0.025) \times 10^3$	100 000	78
40 000	1.01	$(8.361 \pm 0.157) \times 10^2$	100 000	68

to ensure that the integration volume was completely enclosed by the sampling domain (Table II). Inspection of Table II shows that for  $\beta \geq 1.0$  the sampling domain appears to completely enclose the integration volume, even when the vibrational energy is 40 000  $\text{cm}^{-1}$ , nearly 10 000  $\text{cm}^{-1}$  greater than the dissociation energy. When  $\beta = 1.0$ , the Monte Carlo sampling is 100% efficient: every sample point lies within the integration region. When  $\beta > 1.0$ , the efficiency is lower, but convergence of the integral is assured, since points that fall on the boundary are guaranteed to be counted correctly. For most of the calculations,  $\beta$  was set equal to 1.01, which assures convergence of the integral without much sacrifice of efficiency.

Table II also indicates the level of uncertainty that is achievable with this simple technique for a given number of trials. For the three-dimensional (3-D) integration carried out for the water molecule at 40 000  $\text{cm}^{-1}$ , a 1% relative standard deviation required 17 532 trials. If 200 000 trials had been used, the relative standard deviation would have been  $\sim 0.3\%$ . This result can be compared roughly to that obtained by Farantos et al.,<sup>6</sup> who used stratified sampling in the 3-D classical integration for ozone with 9800  $\text{cm}^{-1}$  of vibrational energy; they achieved  $\sim 0.3\%$  relative standard deviation by calculating  $\sim 200\,000$  trials and using more than 150 "strata". This rough comparison shows that the present simple method gives results of high precision, without the necessity for stratified sampling. If the present simple method were to be employed with a stratified sampling scheme, even greater precision could be achieved with a fixed number of trials.

**Nonseparable Anharmonic Oscillators.** These calculations were carried out by using all of the anharmonicities. The sums of vibrational states for nonseparable  $\text{H}_2\text{O}^{11}$  and  $\text{CH}_2\text{O}^{12}$  are significantly larger than the corresponding harmonic and anharmonic separable molecules, as shown in Figures 3 and 4. Although each of these molecules shows significant "local mode" character, the couplings among all of the vibrational modes are quite significant. Couplings between the C-H stretching modes can be incorporated into a local mode description<sup>18</sup> that is more accurate than the "separable model" employed in this paper, but the local mode model still neglects couplings between bends and stretches, which are of fundamental importance in, for example, isomerization reactions.

It is clear from the comparisons in Figure 3 that harmonic models give good approximations (factors of 2) to the full, nonseparable descriptions, even at high energy and for strongly anharmonic and coupled molecules. Thus, for fitting RRKM transition states (with unknown frequencies) to experimental data for a restricted temperature or energy range, little is gained by employing the coupled model, unless the potential energy surface is known. Otherwise, the unknown harmonic frequencies can be "adjusted" to give agreement with the data. Furthermore, the computational speed of the Monte Carlo technique is far less than that of the Beyer-Swinhart and Stein-Rabinovitch algorithms.

In this paper, we have considered only discrete vibrational states, based on spectroscopic constants. For this purpose, eq 14 describes the sampling boundary. For other degrees of freedom and other intermode coupling schemes, eq 14 must be replaced by other expressions, which may make evaluation of the sampling boundary more difficult. In principle, the methods described here can be extended to any arbitrary molecular model, including classical descriptions. Several groups have employed anharmonic coupling schemes in classical models of molecules and transition states.<sup>19</sup>

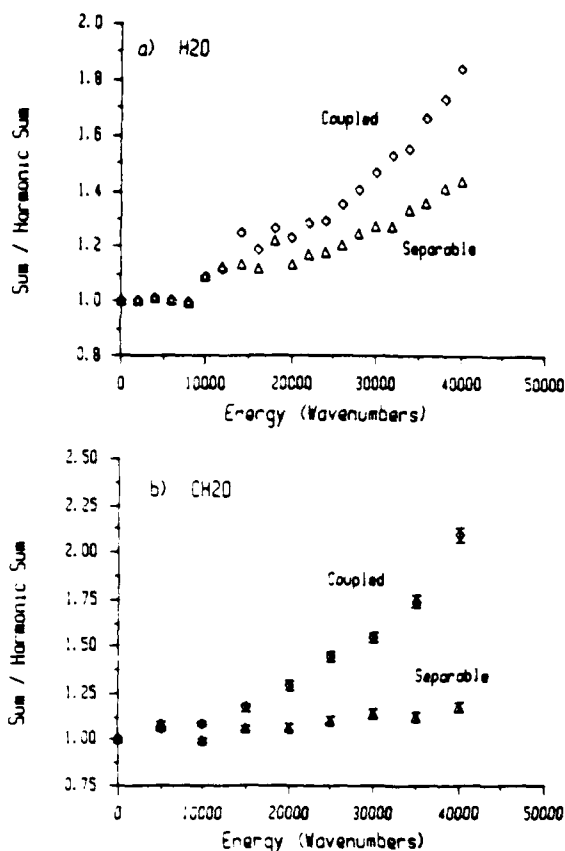


Figure 3. Influence of anharmonicity and coupling for (a) water and (b) formaldehyde.

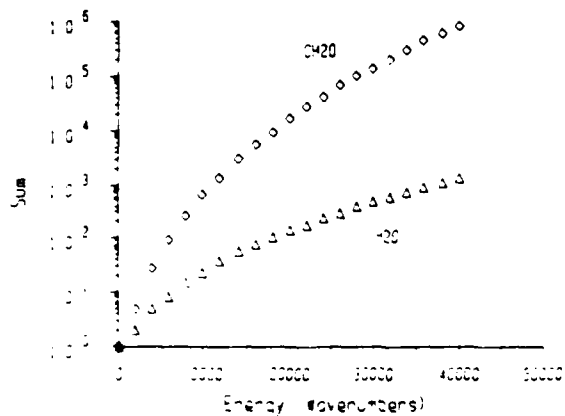


Figure 4. Sums of states for nonseparable anharmonic oscillator models.

In future work, such models will be treated with the Monte Carlo method described here.

For theoretical calculations of rate constants from potential energy surfaces, where the off-diagonal couplings are known, the Monte Carlo technique gives highly accurate sums of states, regardless of the type of degree of freedom or how it is coupled to other motions of the molecule. Harmonic models are simply not adequate, since they give sums of states that differ significantly from the nonseparable model. The mistaken use of harmonic models could lead to significant misinterpretations, if tunneling, avoided crossings, or some other nonclassical process is invoked.

In general, open reaction channels introduce dramatic anharmonic coupling, which is usually nonseparable; accurate calculations require nonseparable models under these circumstances.

(19) For example, see: (a) Bhuiyan, L. B.; Hase, W. L. *J Chem Phys* 1983, 79, 5052. (b) Wardlaw, D. M.; Marcus, R. A. *J Chem Phys* 1985, 83, 1462 and references cited therein.

Thus, the Monte Carlo techniques may find wide use in describing van der Waals complexes, energy-transfer "complexes", and transition-state properties at and above the critical energies for reaction, especially when the reaction is studied over wide energy and temperature ranges.

#### Conclusions

A general Monte Carlo technique for high-dimensional integrals is described and applied to calculations of sums of states for nonseparable anharmonic molecules. The method can be applied to sampling domains with complicated boundaries, and it has an efficiency that can equal unity in realistic applications. When applied to the spectroscopically determined properties of real molecules, the results show that the calculational technique gives accurate results and relative standard deviations comparable with

those obtained by a modern stratified sampling method, which is much more complicated to implement.

The sums of states for the nonseparable vibrations of  $\text{H}_2\text{O}$  and  $\text{CH}_2\text{O}$  are significantly different from those for the separable vibrations. Harmonic vibrations are probably acceptable for empirically fitting RRKM models to experimental data, but theoretical calculations of rate constants and lifetimes must properly account for the nonseparable characteristics of the potential energy surface. The Monte Carlo technique described here is suitable for such calculations.

*Acknowledgment.* Conversations with William L. Hase and William R. Martin are gratefully acknowledged. This work was funded, in part, by the Department of Energy, Office of Basic Energy Sciences, and by the Army Research Office

APPENDIX B.

# Vibrationally excited populations from IR-multiphoton absorption.

## II. Infrared fluorescence measurements<sup>a)</sup>

Jean-Michel Zellweger

*Department of Chemical Kinetics, Chemical Physics Laboratory, SRI International, Menlo Park, California 94025*

Trevor C. Brown

*Department of Chemical Engineering, University of Adelaide, Box 498, G. P. O., Adelaide, South Australia 5001*

John R. Barker<sup>b)</sup>

*Department of Atmospheric and Oceanic Science, Space Physics Laboratory, University of Michigan, Ann Arbor, Michigan 48109-2143*

(Received 31 July 1985; accepted 6 September 1985)

Infrared emission spectra were obtained for 1, 1, 2-trifluoroethane (TFE) excited by infrared multiphoton absorption ( $1079.85 \text{ cm}^{-1}$ ). The emission features show that the HF reaction product is formed in vibrational states up to about  $v = 3$ . Furthermore, emission attributed to  $\text{F}-\text{C}\equiv\text{C}-\text{H}$  was observed near  $3320 \text{ cm}^{-1}$ , indicating that the difluoroethylene primary products of TFE decomposition undergo secondary photolysis; since the difluoroethylene products at room temperature do not absorb laser light, they must be formed vibrationally excited. The emission from the C-H stretch modes of TFE was readily identified near  $2980 \text{ cm}^{-1}$  and the emission intensity was obtained as a function of laser fluence. These data are in excellent agreement with predictions based on the theoretical expression for fluorescence intensity and the reconstructed populations determined by the Master Equation calculations described in the preceding paper. These results provide additional support for the accuracy of the reconstructed population distributions and for the theory relating infrared fluorescence intensity to total vibrational energy in polyatomic molecules.

### INTRODUCTION

In the preceding paper,<sup>1</sup> results from two experimental techniques were used in conjunction with a Master Equation model<sup>2</sup> to determine the population distributions produced by infrared multiphoton absorption (MPA). The experimental techniques used were optoacoustic measurement of absorbed laser energy<sup>3</sup> and VLP $\Phi$ <sup>4</sup> measurement of infrared multiphoton decomposition (IRMPD) yields.<sup>5</sup> Although these techniques enabled us to reconstruct the approximate population distributions produced by MPA, they do not probe directly the population of molecules excited to energies below the decomposition threshold.

*In situ* experimental techniques that directly monitor the vibrational energies of highly vibrationally excited molecules in their electronic ground states are relatively scarce. For small molecules, laser induced fluorescence<sup>6</sup> and Raman spectroscopic methods<sup>7</sup> are appropriate, but for large molecules with high densities of states, UV absorbance<sup>8-11</sup> and infrared fluorescence<sup>12-14</sup> (IRF) have proved to be effective. Each of these methods requires a calibration curve that relates the observed signal to the vibrational energy.

For the IRF techniques, the calibration curve relating intensity to vibrational energy can be calculated from vibrational spectroscopic theory, or it can be derived from experi-

ments. An important motivation for the present experiments is to test the theoretical predictions of IRF intensity against measurements performed using MPA to produce known populations of excited molecules. Validation of the theoretical expression in the present experiments supports theoretical calculations of infrared emission spectra of highly excited molecules. Such calculations find many uses, including simulations of IRF from interstellar molecules excited by absorption of starlight.<sup>15</sup>

The experimental approach in the present work is to obtain time- and wavelength-resolved IFF data as functions of laser fluence and collider-gas pressure. By extrapolating the decay curves to the time origin, the initial IRF intensity can be compared to that predicted by vibrational spectroscopic theory and the Master Equation described in paper I. In the third paper of this series,<sup>16</sup> the calibration curve is used to monitor collisional energy transfer and determine the energy and temperature dependences of the energy transfer step size.

### EXPERIMENTAL

Most of the experimental details are described in paper I. Briefly, high power TEA  $\text{CO}_2$  lasers operating on the  $9.6 \mu\text{m}$   $R(22)$  line ( $1079.85 \text{ cm}^{-1}$ ) were used to excite 1, 1, 2-trifluoroethane. Laser energy was measured with a volume-absorbing calorimeter and fluence was calculated from the measured energy and the laser beam cross-sectional area. Gas pressures were measured with a capacitance manometer.

<sup>a)</sup> All of the experimental work was carried out at SRI International and was supported by the U. S. Army Research Office

<sup>b)</sup> Address correspondence to this author

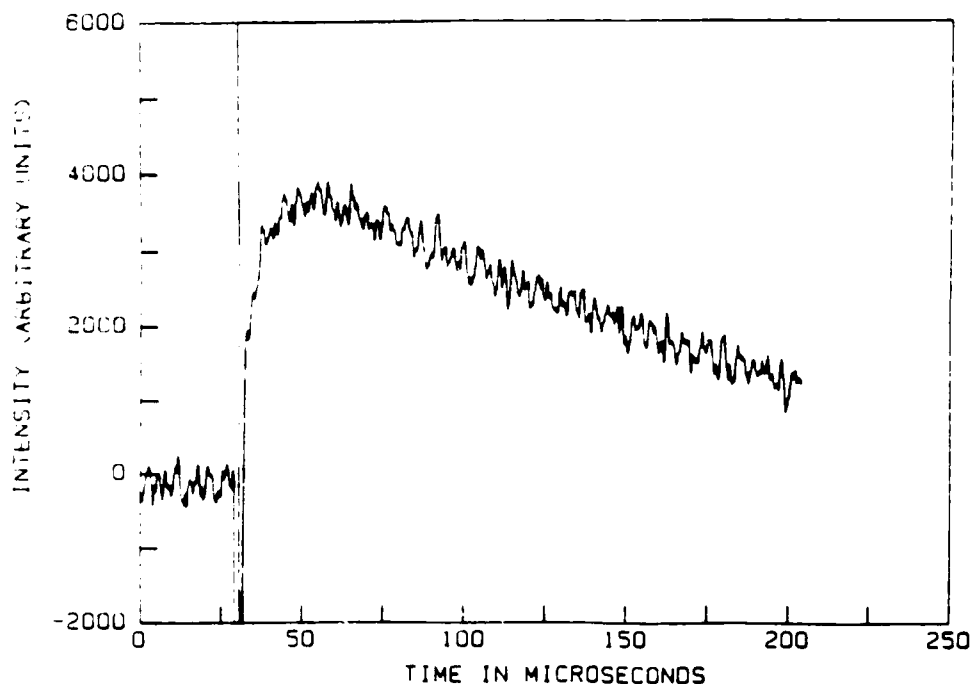


FIG. 1 Infrared fluorescence decay curve. 20 mTorr TFE and 20 mTorr argon,  $\Phi = 1.89 \text{ J cm}^{-2}$ , 143 laser shots,  $3815 \text{ cm}^{-1}$ .

The cell used for the IRF experiments was the same as that used for the optoacoustic measurements in paper I. The fluorescence was viewed through a KCl side window by a liquid nitrogen cooled two-color infrared detector (Infrared Associates, Inc.), which consists of an InSb detector overlying a HgCdTe photodiode. Each detector layer is equipped with a separate preamplifier and biasing circuit. The InSb layer is sensitive from 1 to  $5.5 \mu\text{m}$ ; at longer wavelengths it is transparent, allowing the HgCdTe detector to respond to wavelengths from  $5.5$  to  $16 \mu\text{m}$ . In the present experiments, only the InSb portion of the detector was used. The original time response of the InSb detector/preamplifier was  $1\text{--}2 \mu\text{s}$ , but it was susceptible to electrical interference from the la-

zers; thus it was modified to give a slower time response ( $5\text{--}6 \mu\text{s}$ ) and less susceptibility, although there is still some evidence of electrical "ringing". With this modification and due to the ringing, accurate measurements were limited to decay rate constants slower than about  $7 \times 10^4 \text{ s}^{-1}$ . The signal from the InSb detector/preamplifier was captured using a transient recorder (Biomation 805) and signal averager (Nicolet 1072) interfaced to a laboratory computer (see paper I for details).

Wavelength resolution was achieved using a three-segment circular variable filter (OCLI) mounted in a custom Dewar with the detector and cooled to  $77 \text{ K}$ . The slits were  $1.5 \text{ mm}$ , giving a resolution of about 2% of the center wave-

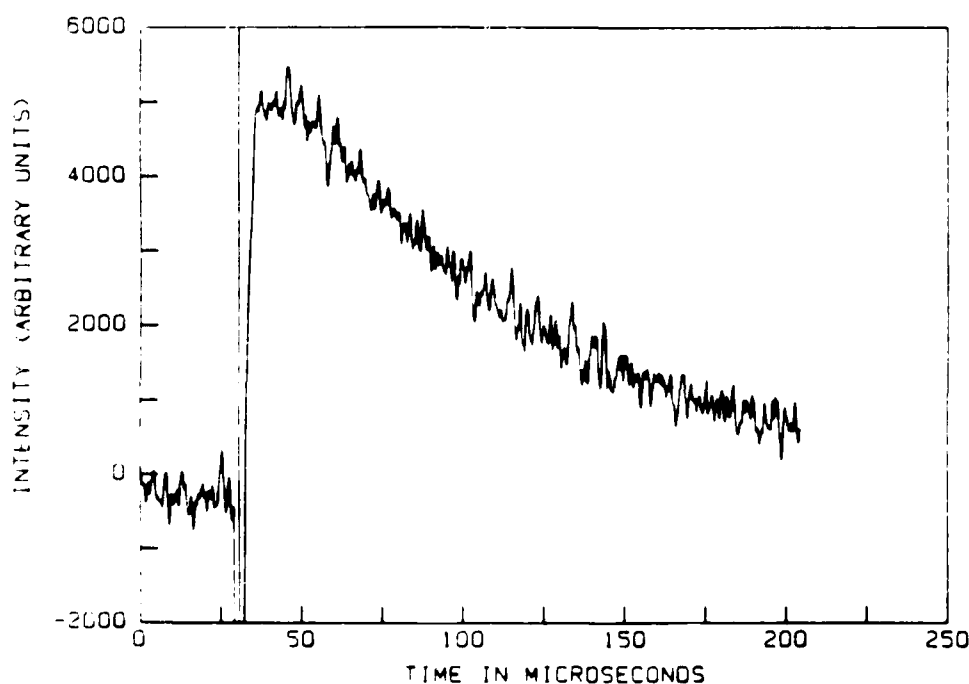


FIG. 2 Infrared fluorescence decay curve. 20 mTorr TFE and 20 mTorr argon,  $\Phi = 1.80 \text{ J cm}^{-2}$ , 253 laser shots,  $3665 \text{ cm}^{-1}$ .

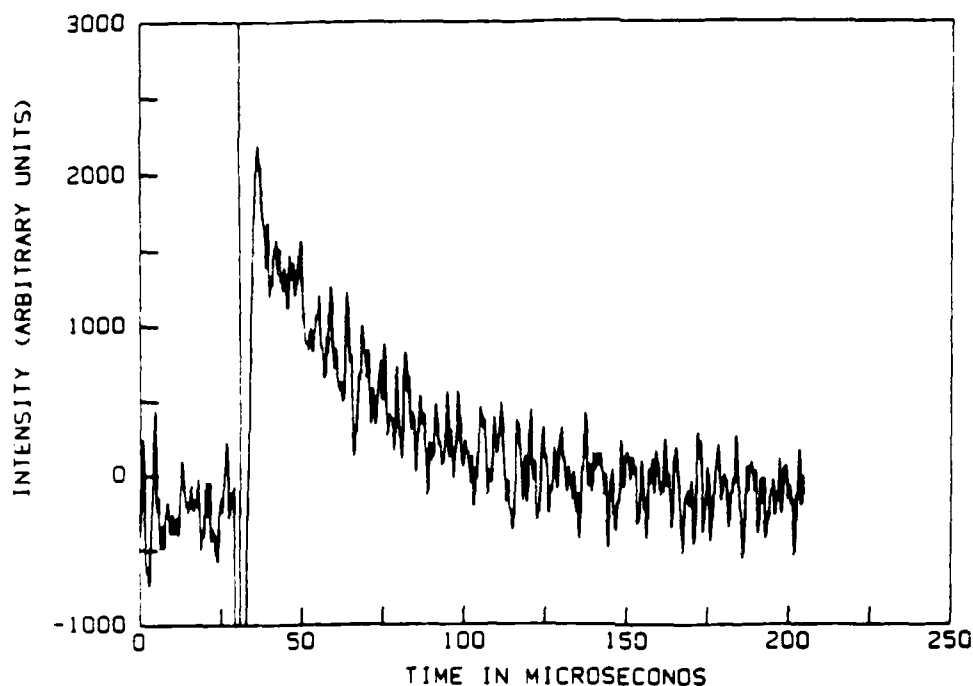


FIG. 3. Infrared fluorescence decay curve. 19 mTorr TFE and 19 mTorr argon,  $\Phi = 1.95 \text{ J cm}^{-2}$ , 121 laser shots, 3020  $\text{cm}^{-1}$ .

length. This resolution is sufficient to distinguish C-H stretch emission bands from HF emission and other interferences. The filter bandpass and relative wavelength calibration (wavelength vs rotation angle) were determined using an infrared spectrometer. Absolute positioning of the rotation angle was achieved by observing the  $\text{CO}_2$  laser line at  $9.26 \mu\text{m}$  and fluorescence from  $\text{CO}_2$  near  $4.2 \mu\text{m}$ . We estimate the absolute wavelength calibration to be accurate to within  $\pm 20 \text{ cm}^{-1}$ .

## RESULTS AND DISCUSSION

A survey of the IRF emission was carried out for wavelengths from about 2000 to  $4000 \text{ cm}^{-1}$  and laser fluences

from 0.6 to  $1.95 \text{ J cm}^{-2}$ . In these experiments, a 1/1 mixture of 1, 1, 2-trifluoroethane (TFE) in argon at a total pressure of 32–40 mTorr flowed slowly through the cell. Argon was added to slow the rates of diffusion and thermal conductivity, and to moderate the temperature excursions. The laser pulse repetition frequency was 0.2–8 Hz, depending on laser fluence, and care was taken not to deplete the TFE by more than a few percent. Depending on signal strength, between 50 and 15 000 laser shots were accumulated for each IRF decay curve to improve the signal/noise ratio.

Fluorescence decay curves were obtained at wavelength intervals of 50–100  $\text{cm}^{-1}$  and a few representative examples are presented in Fig. 1–3. Figure 3 shows a relatively simple exponential decay, while Figs. 1 and 2 show more complicat-

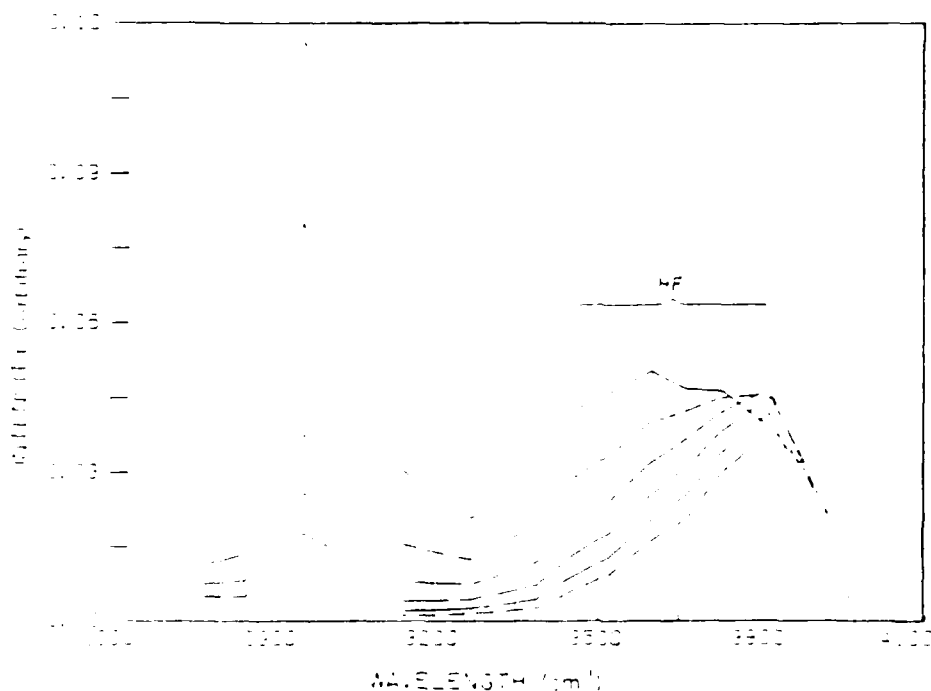


FIG. 4. Time-resolved infrared emission spectrum. 20 mTorr TFE and 20 mTorr argon,  $\Phi = 0.59 \text{ J cm}^{-2}$ , estimated uncertainties are  $\pm 10\%$ . The top solid line is for  $3 \mu\text{s}$  following the laser pulse and each successive line is for additional  $10 \mu\text{s}$  delay times.

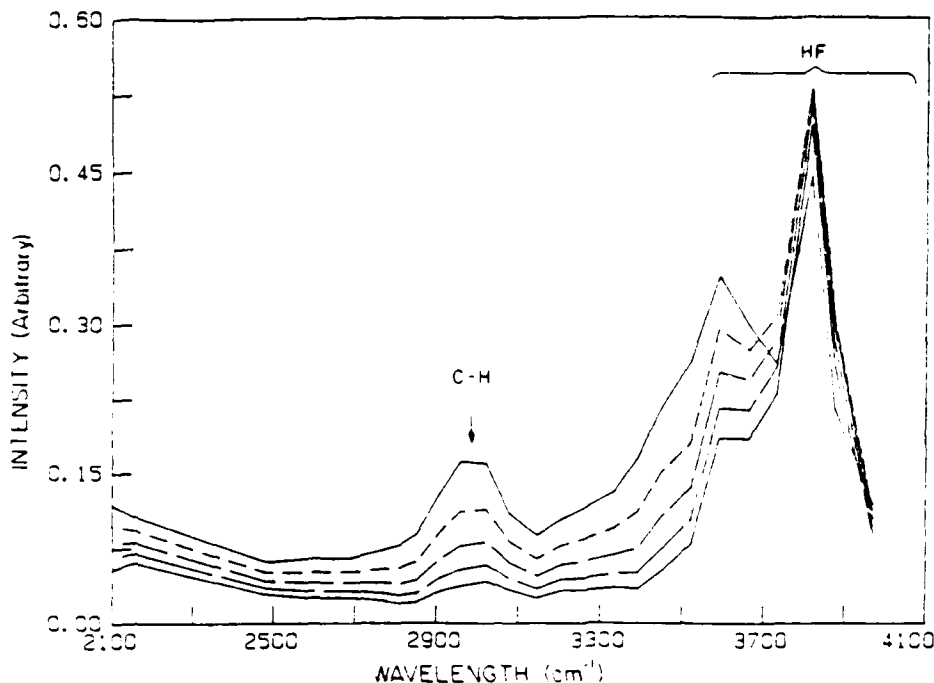


FIG. 5. Time-resolved infrared emission spectrum. 20 mTorr TFE and 20 mTorr argon,  $\Phi = 1.17 \text{ J cm}^{-2}$ , estimated uncertainties are  $\pm 10\%$ . Note the different wavelength scale and see Fig. 4 for key.

ed behavior that is evidence for a collisional cascade. All of the decay curves were individually least-squares fitted by sums of exponentials. By combining the fitted results, we obtained the time- and wavelength-resolved spectra presented in Figs. 4–6, which correspond to low, medium, and high laser fluences, respectively.

Inspection of Figs. 4–6 reveals three distinct spectroscopic features at 2980, 3320, and 3500–3800  $\text{cm}^{-1}$ ; in addition Fig. 5 shows continuum emission between 2100 and 2500  $\text{cm}^{-1}$ , which may be due to the so-called "quasicontinuum",<sup>17</sup> which consists of overtone and combination bands.

The intensity of the broad feature near 3800  $\text{cm}^{-1}$  in-

creases dramatically with laser fluence. The wavelength corresponds to that of the *P* branch of HF, which is a primary reaction product<sup>18</sup>; the wavelength range of the CVF is not sufficient to observe the *Q* branch. This feature changes width and center frequency as a function of time, indicating that several vibrational levels of HF are initially formed in the decomposition of TFE and a vibrational cascade ensues. The detailed shapes of the decay curves in Figs. 1 and 2 are explained by the shift and broadening of the 3800  $\text{cm}^{-1}$  feature. Comparisons of the observed spectra and those for excited HF reported, or discussed in the literature<sup>19</sup> indicate that levels up to about  $v = 3$  are significantly populated in

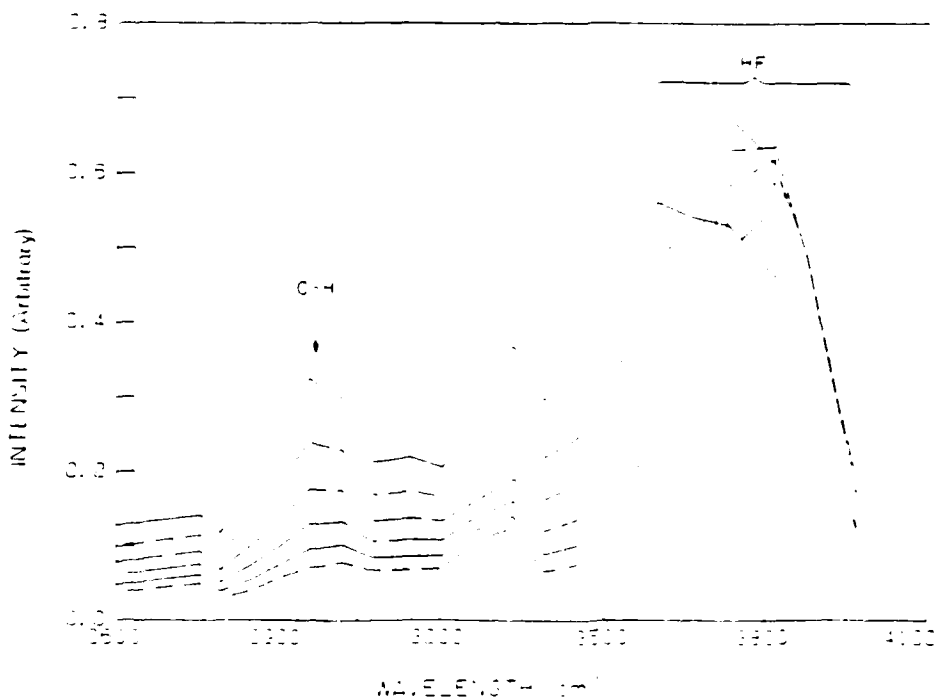
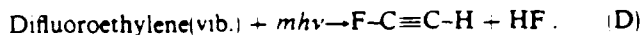
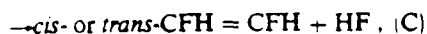
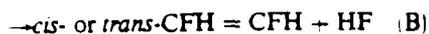
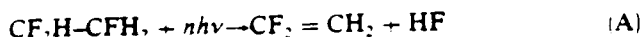


FIG. 6. Time-resolved infrared emission spectrum. 20 mTorr TFE and 20 mTorr argon,  $\Phi = 1.95 \text{ J cm}^{-2}$ , estimated uncertainties are  $\pm 10\%$ . See Fig. 4 for key.

the decomposition reaction. A more detailed analysis is beyond the scope of the present work.

The origin of the feature at  $3320\text{ cm}^{-1}$  is uncertain, but it only appears at very high fluences and is about the same frequency as the C-H stretching mode in acetylene.<sup>20</sup> Thus, we tentatively conclude that it arises from vibrationally excited F-C≡C-H produced by secondary photolysis of difluoroethylene products from the primary dissociation:



The secondary photolysis [process (D)] can only occur with vibrationally excited molecules, because the room temperature difluoroethylene products do not absorb at the laser wavelength, as discussed in paper I. It is interesting to note, then, that both products of the photolysis must contain significant amounts of vibrational energy. Because of the strained three- and four-center cyclic transition state structures, it is expected that vibrationally excited HF and difluoroethylene will be produced, but the extent of excitation and the apportionment of energy varies, depending on the particular reaction channel.<sup>18</sup> For example, the slightly higher energy three-center pathway (C) requires isomerization of the carbene primary product to form difluoroethylene and the difluoroethylene produced by this channel is apportioned more vibrational excitation than the four-center channels.

The spectroscopic feature at  $2980\text{ cm}^{-1}$  corresponds to the C-H stretching modes in TFE.<sup>21</sup> The C-H stretching modes in *cis*- and *trans*-difluoroethylene have frequencies<sup>20</sup> near  $3100\text{ cm}^{-1}$  and cannot contribute to the  $2980\text{ cm}^{-1}$  feature. The monotonic decay curves at this frequency (see Fig. 3) indicate relatively simple collisional deactivation of

the excited TFE and they can be accurately fitted with a single exponential decay. The empirical fitting on the decay curves is used in the present work only for the purpose of extrapolation to obtain the initial intensity; collisional deactivation of TFE is discussed in paper III.<sup>16</sup> The experimental IRF decay curves for  $2980\text{ cm}^{-1}$  were fitted by a single exponential with the Bevington version of the Marquardt nonlinear least squares algorithm.<sup>22</sup> The first  $6\text{ }\mu\text{s}$  of the decay following the laser pulse was neglected (see above) and the least-squares result was extrapolated to  $t = 0$  in order to obtain the initial IRF intensities. The initial intensities were normalized according to the partial pressure of TFE, and the results are presented vs laser fluence in Fig. 7.

For comparison with the experimental results, the IRF intensity was calculated by using the population distributions reconstructed in paper I and the theoretical expression for the microcanonical IRF intensity. The theoretical expression relating IRF intensity to vibrational energy in polyatomic molecules has been discussed elsewhere in detail.<sup>2,12,13</sup> The expression is written

$$I(E) = N_e \times \sum_{i=1}^{\text{Modes}} hv_i A_i^{1,0} \sum_{v=1}^{v_{\text{max}}} v \rho_{s-1}(E - hv_i) / \rho_s(E), \quad (1)$$

where  $N_e$  is the number of excited molecules,  $A_i^{1,0}$  is the Einstein coefficient for emission from the fundamental of the  $i$ th mode,  $v$  is the occupation number of the  $i$ th mode,  $v_{\text{max}}$  is the maximum occupation number for vibrational energy  $E$ ,  $\rho_s(E)$  is the density of vibrational states for all  $s$  vibrational modes, and  $\rho_{s-1}(E - hv_i)$  is the density of states for the  $s - 1$  modes, not including the emitting mode and the energy contained in it.

Briefly, the theoretical expression is based on the fundamental relationship between IRF intensity and vibrational quantum number,<sup>23</sup> and it incorporates two assumptions: (1) the harmonic oscillator approximation relating Einstein coefficients for higher vibrational levels to that for the fundamental and (2) the ergodic assumption, which states that the vibrational energy is statistically distributed among the vi-

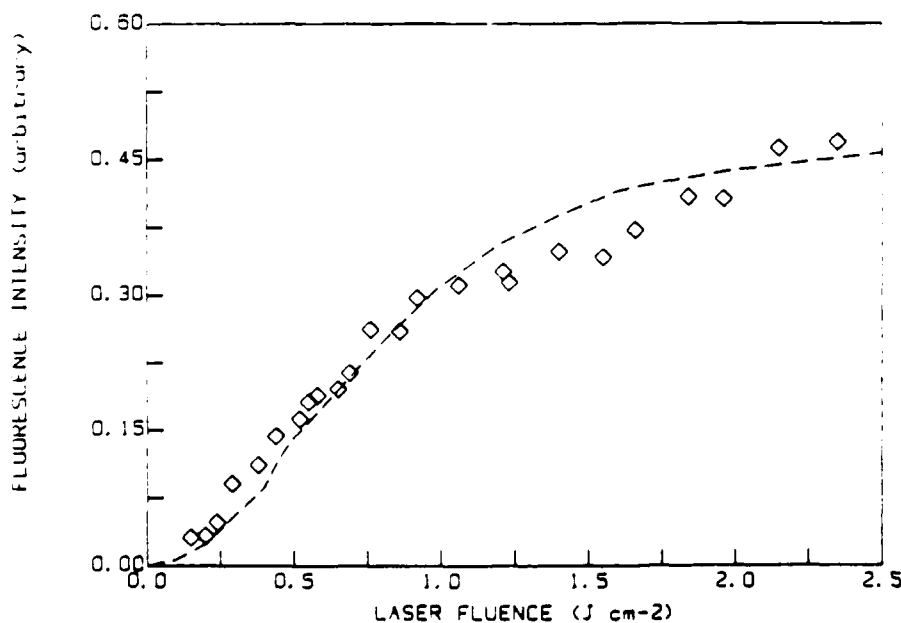


FIG. 7 Infrared fluorescence from TFE C-H modes. Diamond symbols are experimental data points (from extrapolation to time = 0) with estimated uncertainties of  $\pm 5\%$ ; dashed line is theoretical prediction scaled to same magnitude as experiments at  $\Phi = 1\text{ J cm}^{-2}$ .

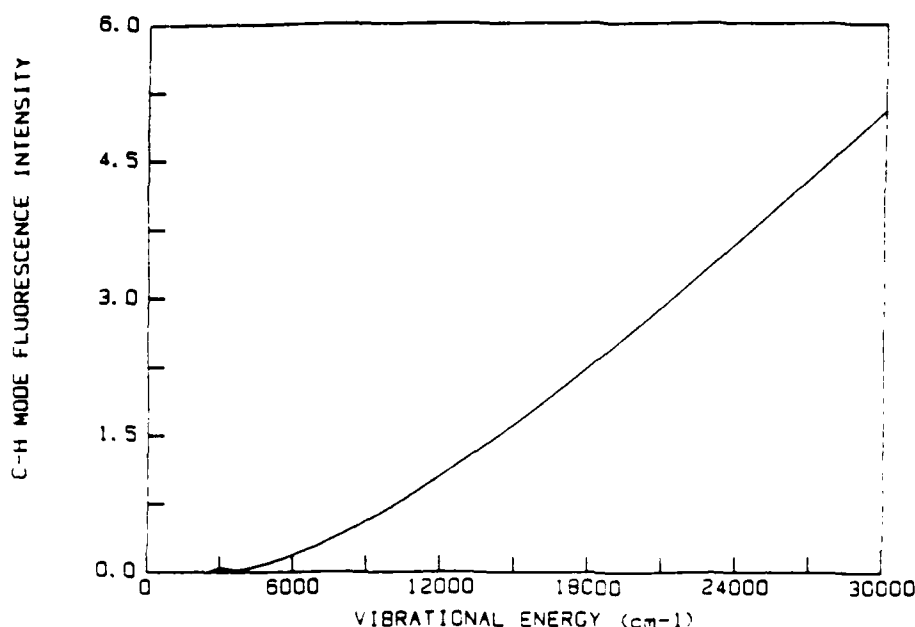


FIG. 8. Microcanonical curve relating IRF from C-H modes to vibrational energy. This curve was calculated using theoretical Eq. (1); see the text for details.

brational modes on the time scale of the fluorescence (microseconds). The accuracy of this expression also relies on the densities of states calculations, which can be carried out using exact-count algorithms.

For the theoretical prediction of IRF intensity vs vibrational energy, the Stein-Rabinovitch method of exact counts<sup>24</sup> was used to obtain the densities of states, based on the vibrational assignments for TFE.<sup>21</sup> The hindered internal rotation was treated as a vibration in these calculations. The Einstein coefficients for the fundamental transitions are not known and they are included in the undetermined scale factor, which also depends on the experiment geometrical configuration, detector sensitivity, amplifier settings, etc. In Fig. 8, the predicted microcanonical dependence of IRF intensity on vibrational energy is presented in arbitrary units.

To compare the predicted IRF intensities with those observed at different laser fluences, the population distributions from paper I were used with the microcanonical IRF intensities to obtain ensemble-averaged IRF intensities vs laser fluence. These theoretical results are shown in Fig. 7 as the dashed line, which has been scaled to match the magnitude of the experimental data at a fluence of  $1.0 \text{ J cm}^{-2}$ . The agreement between experiment and theory is excellent.

The excellence of the agreement between experiment and theory may be viewed in several ways. If Eq. (1) is accepted as accurate, the agreement provides additional support for the reconstructed population distributions obtained in paper I. This is a legitimate point of view in that Eq. (1) has been successfully tested in several other systems on other molecules,<sup>12,13</sup> supporting the inference that it should accurately describe IRF in the molecule TFE. The other point of view is that Eq. (1) must be tested by experiment, despite the elegance of its derivation. The reconstructed population distributions are derived from experiments in paper I and therefore the experiments reported here provide an experimental test and demonstration of the accuracy of Eq. (1), when applied to TFE.

Either of these points of view leads to the conclusion

that the Master Equation from paper I and Eq. (1) constitute a self-consistent description of the results from three independent experimental techniques. Considering the highly constrained parametrization of the Master Equation as described in paper I and the fact that Eq. (1) accurately describes IRF in other systems as well as in this one, we conclude that the reconstructed population distributions are good representations of the actual distributions and that IRF can be confidently used to monitor vibrational energy in TFE excited by multiphoton absorption. This technique is used in paper III to determine energy-transfer properties of TFE.

#### ACKNOWLEDGMENTS

The authors gratefully acknowledge financial support from the U. S. Army Research Office. JMZ acknowledges a fellowship from the Swiss Fonds National, and TCB thanks K. D. King at the University of Adelaide for his support and encouragement. Many of the numerical calculations were carried out in the Chemical Physics Laboratory at SRI using the VAX computing facility, which was provided by a grant from the National Science Foundation; thanks go to Dave Heustis of SRI for his assistance with the least-squares fitting routines. The authors are happy to acknowledge the helpful conversations with D. W. Setser, who also provided technical information on several molecules studied in his laboratory.

<sup>1</sup>J. M. Zellweger, T. C. Brown, and J. R. Barker, *J. Chem. Phys.* **83**, 6251 (1985).

<sup>2</sup>(a) J. R. Barker, *Chem. Phys.* **77**, 301 (1983); (b) J. R. Barker and R. E. Golden, *J. Phys. Chem.* **88**, 1012 (1984).

<sup>3</sup>(a) R. D. Bates, Jr., G. W. Flynn, and J. K. Knudson, *J. Chem. Phys.* **53**, 3621 (1970); (b) *Opto-Acoustic Spectroscopy and Detection*, edited by Y. H. Pao (Academic, New York, 1977); (c) N. Presser, J. R. Barker, and R. J. Gordon, *J. Chem. Phys.* **78**, 2163 (1983); (d) J. R. Barker, L. Brouwer, R. Patrick, M. Rossi, P. L. Trevor, and D. M. Golden, *Int. J. Chem. Kinet.* (in press).

<sup>4</sup>J. S. Chang, J. R. Barker, J. E. Davenport, and D. M. Golden, *Chem.*

- Phys. Lett. **60**, 385 (1979).
- <sup>17</sup>(a) D. M. Golden, M. J. Rossi, A. C. Baldwin, and J. R. Barker, *Acc. Chem. Res.* **L4**, 56 (1981); (b) M. J. Rossi, J. R. Barker, and D. M. Golden, *J. Chem. Phys.* **76**, 406 (1982).
- <sup>18</sup>J. L. Kinsey, *Annu. Rev. Phys. Chem.* **28**, 349 (1977).
- <sup>19</sup>A. G. Robiette and J. L. Duncan, *Annu. Rev. Phys. Chem.* **34**, 245 (1983).
- <sup>20</sup>(a) H. Hippler, J. Troe, and H. J. Wendelken, *Chem. Phys. Lett.* **84**, 257 (1981); (b) *J. Chem. Phys.* **78**, 6709 (1983); (c) **78**, 6718 (1983).
- <sup>21</sup>(a) J. E. Dove, H. Hippler, and J. Troe, *J. Chem. Phys.* **82**, 1907 (1985); (b) H. Hippler, D. Nahr, and J. Troe (to be published).
- <sup>22</sup>N. Nakashima and K. Yoshihara, *J. Chem. Phys.* **79**, 2727 (1983).
- <sup>23</sup>T. Ichimura, Y. Mori, N. Nakashima, and K. Yoshihara, *J. Chem. Phys.* **83**, 117 (1985).
- <sup>24</sup>J. F. Durana and J. D. McDonald, *J. Chem. Phys.* **64**, 2518 (1976).
- <sup>25</sup>(a) G. P. Smith and J. R. Barker, *Chem. Phys. Lett.* **78**, 253 (1981); (b) M. J. Rossi and J. R. Barker, *ibid.* **85**, 21 (1982); (c) J. R. Barker, M. J. Rossi, and J. R. Pladziewicz, *ibid.* **90**, 99 (1982); (d) M. J. Rossi, J. R. Pladziewicz, and J. R. Barker, *J. Chem. Phys.* **78**, 6695 (1983); (e) J. R. Barker, *J. Phys. Chem.* **88**, 11 (1984); (f) J. R. Barker and R. E. Golden, *ibid.* **88**, 1012 (1984); (g) W. Forst and J. R. Barker, *J. Chem. Phys.* **83**, 124 (1985).
- <sup>26</sup>For example, see J. W. Hudgens and J. D. McDonald, *J. Chem. Phys.* **76**, 173 (1982).
- <sup>27</sup>L. J. Allamandola, A. G. G. M. Tielens, and J. R. Barker, *Astrophys. J.* **290**, L25 (1985); L. J. Allamandola, A. G. G. M. Tielens, and J. R. Barker manuscript in preparation.
- <sup>28</sup>J. M. Zellweger, T. C. Brown, and J. R. Barker, *J. Phys. Chem.* (to be published).
- <sup>29</sup>For reviews of infrared multiphoton ideas, see (a) N. Bloembergen and E. Yablonovitch, *Phys. Today* **31**, 32 (1978); (b) P. A. Schultz, A. S. Sudbo, D. J. Krajnovich, H. S. Kwok, Y. R. Shen, and Y. T. Lee, *Annu. Rev. Phys. Chem.* **30**, 379 (1979); (c) M. F. Goodman, J. Stone, and E. Thiele, in *Multiple-Photon Excitation and Dissociation of Polyatomic Molecules*, edited by C. D. Cantrell (Springer, Berlin, 1980); (d) J. L. Lyman, G. P. Quigley, and O. P. Judd, *ibid.*; (e) D. S. King, *Dynamics of the Excited State*, edited by K. P. Lawley (Wiley, New York, 1982), p. 105.
- <sup>30</sup>B. E. Holmes, D. W. Setser, and G. O. Pritchard, *Int. J. Chem. Kinet.* **8**, 215 (1976), and references therein.
- <sup>31</sup>(a) C. R. Quick, Jr. and C. Wittig, *Chem. Phys.* **32**, 75 (1978); (b) G. A. West, R. E. Weston, Jr., and G. W. Flynn, *ibid.* **35**, 275 (1978); (c) C. R. Quick, Jr. and C. Wittig, *J. Chem. Phys.* **72**, 1694 (1980); (d) J. F. Caballero and C. Wittig, *Chem. Phys. Lett.* **82**, 63 (1981).
- <sup>32</sup>(a) T. Shimanouchi, *Tables of Molecular Vibrational Frequencies*, Natl. Stand. Ref. Data Serv. Natl. Bur. Stand. 39 (U.S. GPO, Washington, D. C., 1972), Vol. 1; (b) T. Shimanouchi, *J. Phys. Chem. Ref. Data* **6**, 993 (1977).
- <sup>33</sup>V. F. Kalasinsky, H. V. Anjaria, and T. S. Little, *J. Phys. Chem.* **86**, 1351 (1982).
- <sup>34</sup>P. R. Bevington, *Data Reduction and Error Analysis for the Physical Sciences* (McGraw-Hill, New York, 1969), p. 237.
- <sup>35</sup>G. Herzberg, *Infrared and Raman Spectra* (Van Nostrand, Princeton, 1945).
- <sup>36</sup>S. E. Stein and B. S. Rabinovitch, *J. Chem. Phys.* **58**, 2438 (1973).

APPENDIX C.

### Vibrationally Excited Populations from IR-Multiphoton Absorption. 3. Energy Transfer between 1,1,2-Trifluoroethane and Argon<sup>†</sup>

Jean-Michel Zellweger,

*Department of Chemical Kinetics, Chemical Physics Laboratory, SRI International,  
Menlo Park, California 94025*

Trevor C. Brown,

*Department of Chemical Engineering, University of Adelaide, G.P.O., Adelaide, South Australia 5001*

and John R. Barker\*

*Department of Atmospheric and Oceanic Science, Space Physics Laboratory, University of Michigan,  
Ann Arbor, Michigan 48109-2143 (Received: July 22, 1985)*

Infrared multiphoton absorption at several laser fluences ( $1079.85 \text{ cm}^{-1}$ ) has been used to generate vibrationally excited 1,1,2-trifluoroethane molecules at energies below the reaction threshold. A technique is demonstrated in which collisional deactivation of the vibrationally excited molecules by argon was monitored with time-resolved infrared fluorescence from the C-H stretch modes. The experimental results were simulated by using a full collisional master equation treatment that incorporated Quack's theory of multiphoton absorption, as parameterized elsewhere for TFE, and a calibration curve relating fluorescence to vibrational energy (previously determined for TFE). When the exponential model for collision transition probabilities was used, the simulations gave  $\langle \Delta E \rangle_d = (200 \pm 20) + (0.005 \pm 0.002)E$ , where  $\langle \Delta E \rangle_d$  is the energy step size ( $\text{cm}^{-1}$ ) for deactivating collisions by argon and  $E$  is the vibrational energy of the excited TFE. The simulations showed that  $\langle \Delta E \rangle_d$  has a significant energy dependence, but it does not exhibit a detectable temperature dependence over the range from about 400 to 1000 K. In the Introduction, current research activities by several workers active in the area of large molecule energy transfer are briefly surveyed.

#### Introduction

Recently, three major questions and several lesser ones have arisen about vibrational energy transfer involving large molecules. These questions are all concerned with  $\langle \Delta E \rangle_d$ , the average amount of energy transferred in deactivating collisions, which is related by microscopic reversibility and detailed balance to  $\langle \Delta E \rangle$ , the average amount of energy transferred in both activating and deactivating collisions.<sup>1</sup> The major questions are concerned with (1) the magnitude of  $\langle \Delta E \rangle_d$ , (2) whether  $\langle \Delta E \rangle_d$  depends on the

vibrational energy of the highly vibrationally excited molecule, and (3) how  $\langle \Delta E \rangle_d$  varies with the collider bath gas temperature. Few energy-transfer systems have been examined in enough detail to address any of these questions and the conflicting results may stem from the different molecules studied, or from undetected experimental artifacts.

One of the best approaches to determining the actual reliability of experimental data is to compare results from several different

<sup>†</sup> All of the experimental work was carried out SRI International.

(1) For an interesting discussion of the relative merits of citing  $\langle \Delta E \rangle$  or  $\langle \Delta E \rangle_d$ , see Gilbert, R. G. *Chem. Phys. Lett.* 1982, 85, 21.

experimental techniques. This was one of the primary motivations of our work on azulene,<sup>2</sup> which employed visible and UV laser photoexcitation to prepare the vibrationally excited molecules at selected energies and time-resolved infrared fluorescence to monitor their collisional deactivation. These experiments on a nonreactive system were intended to test and extend the large body of energy-transfer data obtained in unimolecular reaction rate studies.<sup>3</sup>

Recently, Hippler, Troe, and co-workers<sup>4</sup> have also investigated photoexcited azulene at one excitation energy, but they monitored the deactivation by time-resolved UV-absorbance techniques and reached slightly different conclusions. Specifically, both studies agree that the magnitudes of  $\langle \Delta E \rangle_d$  in the azulene system are somewhat smaller for efficient colliders than estimated on the basis of unimolecular reaction rate studies, but Hippler, Troe, and co-workers concluded that  $\langle \Delta E \rangle_d$  is essentially independent of vibrational energy content, contrary to our conclusions, but in agreement with their own work on other molecules.<sup>5</sup>

Not all UV-absorbance experiments give energy-independent values for  $\langle \Delta E \rangle_d$ . Experiments by Troe and co-workers<sup>6</sup> on triatomic molecules give values for  $\langle \Delta E \rangle_d$  that depend dramatically on internal energy. Also, in time-resolved UV-absorbance experiments carried out by Nakashima and Yoshihara on benzene<sup>7</sup> and hexafluorobenzene,<sup>8</sup> the results indicate that  $\langle \Delta E \rangle_d$  is directly proportional to internal energy. Thus experiments using infrared fluorescence on these molecules would provide another useful comparison.

In a second controversy concerning the properties of  $\langle \Delta E \rangle_d$ , different studies have arrived at significantly different conclusions about its temperature dependence. It was concluded on the basis of infrared fluorescence experiments<sup>2a</sup> that  $\langle \Delta E \rangle_d$  shows a slight decrease in magnitude as the collider bath gas temperature is raised. On the other hand, multiple-channel unimolecular reaction studies indicate a very strong decrease in magnitude of  $\langle \Delta E \rangle_d$  with temperature,<sup>9</sup> while UV-absorbance experiments indicate a weak temperature dependence that can change sign depending on the efficiency of the collider.<sup>10</sup> There is no clear explanation for these differences, and new experimental techniques may help to resolve the conflicts.

In a number of different laboratories, new experimental techniques for energy-transfer studies are under development. For example, photoexcitation based on laser pumping of high overtones of the C-H stretching vibrations in potentially reactive molecules has recently been applied in efforts to determine energy-transfer properties.<sup>11,12</sup> Also, several versions of crossed molecular beam experiments are under study in at least three different laboratories.<sup>13-15</sup> Time-resolved optoacoustic methods also show promise

for making contributions to our knowledge of energy transfer involving large molecules.<sup>16</sup> In addition, the disposal of vibrational energy<sup>2c</sup> in the energy-transfer act is being investigated by cold-gas-filter experiments<sup>17</sup> and by time-resolved laser diode absorption measurements.<sup>18</sup> The development and application of these techniques promise to improve vastly knowledge of energy transfer. In the following sections, we will describe the use of infrared multiphoton absorption (MPA) to prepare ensembles of vibrationally excited molecules, which can be monitored by infrared fluorescence (IRF).

### Multiphoton Absorption/Infrared Fluorescence Technique

Infrared multiphoton absorption is fairly general, in that many molecules absorb light from high-power CO<sub>2</sub> lasers. A large fraction of the irradiated molecules are excited by the laser light, but the resulting distribution function is broad and must be characterized, as in the first paper of this series.<sup>19</sup> The earliest applications of the infrared pumping technique analyzed the effects of pressure on multiphoton dissociation yields.<sup>20,21</sup> The analysis is quite complex, because the laser pulse shape and the extreme temperature excursions after the pulse both play important roles.<sup>21,22</sup> Moreover, the interpretation depends critically on accurate knowledge of the specific unimolecular rate constants, which must be determined in separate experiments. Nonetheless, the energy-transfer results showed considerable promise.

The present energy-transfer experiments differ from the earlier dissociation yield techniques in several important ways. The most important difference is that the energy-transfer measurements do not depend on reaction yield measurements, but on infrared fluorescence from nonreacting molecules. Also, milder conditions are used, leading to much smaller temperature excursions, easing interpretations of the results. There is the added benefit that the laser pulse shape is not important in the data analysis and unimolecular rate parameters need not be known with great accuracy. However, the dependence of infrared fluorescence intensity on internal vibrational energy must be known from experiment or from theory.<sup>23</sup> In the second paper of this series, the theoretical expression relating IRF intensity to vibrational energy was compared to experimental results obtained from infrared multiphoton absorption, and the comparison showed very good agreement.<sup>24</sup> Thus, the basis for energy-transfer experiments has been established.

The approach in these experiments is to use multiphoton absorption to prepare nonreactive ensembles of vibrationally excited 1,1,2-trifluoroethane (TFE) molecules (the initial population distributions are known with good accuracy, based on the results of paper 1). The collisional deactivation of the excited molecules is monitored by time-resolved IRF from the C-H stretching modes. By varying the gas pressure, the deactivation rate can be varied systematically, and by changing gas composition, the temperature excursions can also be controlled. Thus, investigation of the effects of laser fluence and of gas composition enables us to determine the dependence of  $\langle \Delta E \rangle_d$  on vibrational energy and on temperature.

Because of the temperature excursions and because the initial population distributions are relatively broad, a master equation treatment is used in data analysis. The master equation implementation used to simulate the experimental data has been de-

(2) (a) Smith, G. P.; Barker, J. R. *Chem. Phys. Lett.* **1981**, *78*, 253. (b) Rossi, M. J.; Barker, J. R. *Chem. Phys. Lett.* **1982**, *85*, 21. (c) Barker, J. R.; Rossi, M. J.; Pladziewicz, J. R. *Chem. Phys. Lett.* **1982**, *90*, 99. (d) Rossi, M. J.; Pladziewicz, J. R.; Barker, J. R. *J. Chem. Phys.* **1983**, *78*, 6695. (e) Barker, J. R. *J. Phys. Chem.* **1984**, *88*, 11. (f) Barker, J. R.; Golden, R. E. *J. Phys. Chem.* **1984**, *88*, 1012. (g) Forst, W.; Barker, J. R. *J. Chem. Phys.* **1985**, *83*, 124.

(3) (a) Tardy, D. C.; Rabinovitch, B. S. *Chem. Rev.* **1977**, *77*, 369. (b) Quack, M.; Troe, J. *Spec. Period. Rep., Chem. Soc.* **1977**, *2*, 175.

(4) (a) Hippler, H. *Ber. Bunsenges. Phys. Chem.* **1985**, *89*, 304. (b) Hippler, H.; Lindemann, L.; Troe, J. *J. Chem. Phys.* **1985**, *83*, 3906.

(5) (a) Hippler, H.; Troe, J.; Wendelken, H. *J. Chem. Phys. Lett.* **1981**, *84*, 257. (b) Hippler, H.; Troe, J.; Wendelken, H. *J. Chem. Phys.* **1983**, *79*, 6709. (c) Hippler, H.; Troe, J.; Wendelken, H. *J. Chem. Phys.* **1983**, *79*, 6718.

(6) (a) Dove, J. E.; Hippler, H.; Troe, J. *J. Chem. Phys.* **1985**, *82*, 1907. (b) Hippler, H.; Nahr, D.; Troe, J., to be submitted for publication.

(7) Nakashima, N.; Yoshihara, K. *J. Chem. Phys.* **1983**, *79*, 2727.

(8) Nakashima, N.; Yoshihara, K. *J. Chem. Phys.*, in press.

(9) (a) Krongauz, V. V.; Rabinovitch, B. S. *J. Chem. Phys.* **1983**, *78*, 3872. (b) Krongauz, V. V.; Rabinovitch, B. S.; Linkaityte-Weiss, E. *J. Chem. Phys.* **1983**, *78*, 5643, and references cited therein.

(10) Heyman, M.; Hippler, H.; Troe, J. *J. Chem. Phys.* **1984**, *80*, 1853.

(11) (a) Chandler, D. W.; Farneth, W. E.; Zare, R. N. *J. Chem. Phys.* **1982**, *77*, 4447. (b) Chuang, M. C.; Baggott, J. E.; Chandler, D. W.; Zare, R. N. *Faraday Discuss., Chem. Soc.* **1982**, *75*, 17. (c) Chandler, D. W.; Miller, J. A. *J. Chem. Phys.* **1984**, *81*, 455. (d) Snavely, D. L.; Zare, R. N., private communication.

(12) Rizzo, T. R.; Crim, F. F. *J. Chem. Phys.* **1982**, *76*, 2754.

(13) Colussi, A. J., private communication.

(14) Oref, I., private communication.

(15) Rabinovitch, B. S., private communication.

(16) Beck, K. M.; Ringwelski, A.; Gordon, R. J. *J. Chem. Phys. Lett.* **1985**, *121*, 529.

(17) Vlahoyannus, Y. P.; Koshi, M.; Gordon, R. J. *J. Chem. Phys.*, in press.

(18) Jalenak, W.; Weston, R. E., Jr.; Sears, T. J.; Flynn, G. J. *J. Chem. Phys.* **1985**, *83*, 6049.

(19) Paper I: Zellweger, J.-M.; Brown, T. C.; Barker, J. R. *J. Chem. Phys.* **1985**, *83*, 6251; this paper describes the photophysics.

(20) Baldwin, A. C.; van den Bergh, H. *J. Chem. Phys.* **1981**, *74*, 1012.

(21) Brown, T. C.; Taylor, J. A.; King, K. D.; Gilbert, R. G. *J. Phys. Chem.* **1983**, *87*, 5214.

(22) Barker, J. R. *J. Chem. Phys.* **1983**, *77*, 301.

(23) Durana, J. F.; McDonald, J. D. *J. Chem. Phys.* **1976**, *64*, 2518.

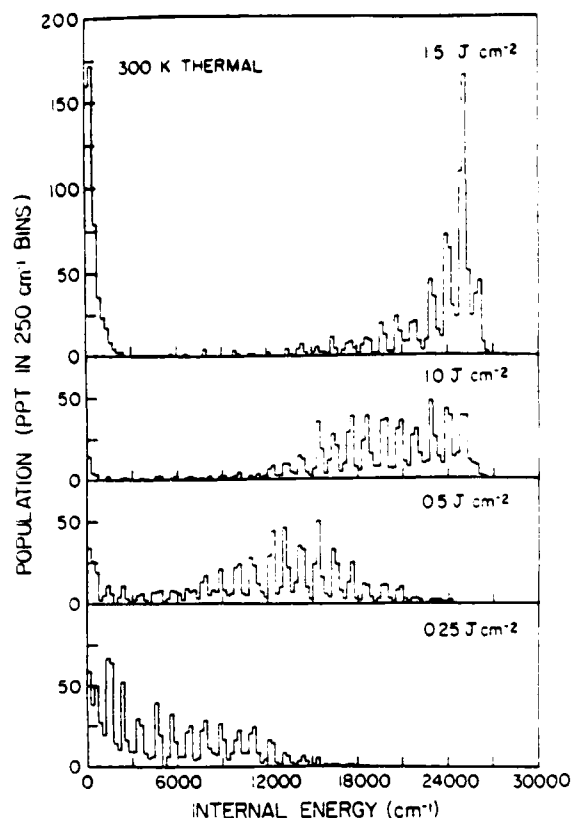


Figure 1. Reconstructed population distributions. These population distributions are from the master equation treatment, as parameterized in paper I. For comparison, the 300 K thermal distribution ( $\times 1/2$ ) is shown in the top panel.

scribed in detail elsewhere.<sup>2f,22</sup> Recent improvements described in paper I consist of using exact-count densities of states, rather than the Whitten-Rabinovitch approximation, and incorporating Quack's theory of infrared multiphoton absorption.<sup>25</sup> Parameterization of the theory to fit infrared multiphoton absorption by TFE allowed us to reconstruct the population distribution produced by a selected laser fluence.<sup>19</sup>

Although the experimental population distributions are not uniquely determined by the master equation simulation approach, the theoretical reconstruction is a good approximation and is used as input in the energy-transfer simulations. It was shown in paper II that the reconstructed populations could be coupled with the theoretical expression for IRF dependence on vibrational energy to accurately predict the observed IRF intensity produced by laser fluences up to about  $2 \text{ J cm}^{-2}$ .<sup>24</sup>

Examples of the reconstructed population distributions for TFE are presented in Figure 1. These populations show the broad distributions often predicted by most models for infrared multiphoton absorption, but there are additional features that are of interest. At low fluences, significant numbers of molecules remain in the initial thermal distribution and are not pumped up the ladder. This feature is a direct consequence of the behavior of Quack case C,<sup>25</sup> which dominates in the sparse density of states region at low energy. At very high fluences, the population distributions tend to "stack up" at high energies and become much narrower. This effect is due to a pumping "bottleneck" caused by the anharmonic shift of the pumped vibrational mode (a C-F stretch).<sup>19</sup> The anharmonicity is large for energies near the reaction threshold, because the electronic hybridization of the carbon

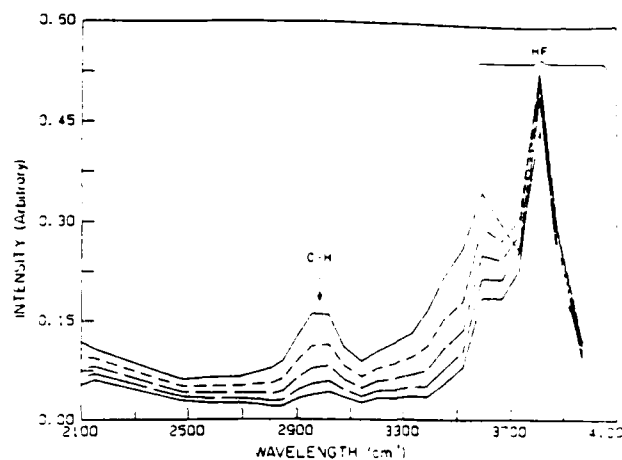


Figure 2. Infrared emission spectra. From the experiments in paper II, these time- and wavelength-resolved curves correspond to about 20 mtorr of TFE diluted in 20 mtorr of Ar and pumped at  $1079.85 \text{ cm}^{-1}$  with a laser fluence of  $1.2 \text{ J cm}^{-2}$ . The first spectrum (top solid line) is  $8 \mu\text{s}$  after the pulse, and each succeeding spectrum occurs  $10 \mu\text{s}$  later.

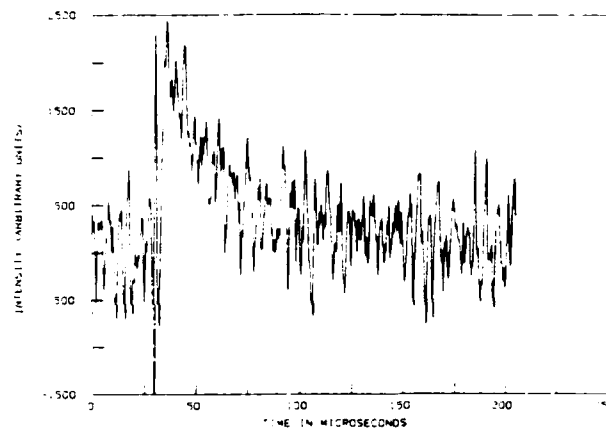


Figure 3. Infrared fluorescence decay curve. Emission at  $2980 \text{ cm}^{-1}$  from 9 mtorr of TFE diluted in 81 mtorr of Ar and pumped with a laser fluence of  $1.07 \text{ J cm}^{-2}$ ; the least-squares decay rate constant is  $(4.09 \pm 0.22) \times 10^4 \text{ s}^{-1}$ .

atoms changes from  $sp^3$  to  $sp^2$  as the molecule reacts by HF molecular elimination.

### Experimental Section

The experimental apparatus and techniques are the same as those used in papers I and II. Briefly, a high-power pulsed  $\text{CO}_2$  laser tuned to the  $1079.85\text{-cm}^{-1}$  transition is used to excite 1,1,2-trifluoroethane (TFE) diluted in argon. Infrared fluorescence from the C-H stretch modes of TFE is used to monitor the collisional deactivation of the excited molecules. The IRF is spectrally isolated with a circular variable filter set at  $2980 \text{ cm}^{-1}$ . The resolution of the filter at this wavelength is about  $60 \text{ cm}^{-1}$ , sufficient to cleanly distinguish the C-H IRF from HF fluorescence and other interferences, as shown in paper II, where time- and wavelength-resolved IRF spectra were obtained; an example is presented in Figure 2. The IRF is monitored by using the InSb portion of a two-color infrared detector (Infrared Associates, Inc.) and the signal is captured with a transient recorder/signal averager interfaced to a laboratory computer. The overall time constant of the detector, amplifiers, and digital electronics is  $1\text{--}2 \mu\text{s}$ , but the first  $4\text{--}6 \mu\text{s}$  of the signal is obliterated by electrical interference from the pulsed laser.

### Results and Discussion

A typical IRF decay is presented in Figure 3, which shows the effect of the electrical interference. This decay curve was obtained with 1030 laser shots and it illustrates that the signals are quite

(24) Paper II: Zellweger, J.-M.; Brown, T. C.; Barker, J. R. *J. Chem. Phys.* 1985, 83, 6261; this paper describes the infrared fluorescence observed.

(25) Quack, M. *Ber. Bunsenges. Phys. Chem.* 1981, 85, 318 [for a treatment that considers fluence-dependent fractionation of pumped and non-pumped molecules, see Jang, J. C.; Setzer, D. W.; Danen, W. C. *J. Am. Chem. Soc.* 1982, 104, 5440].

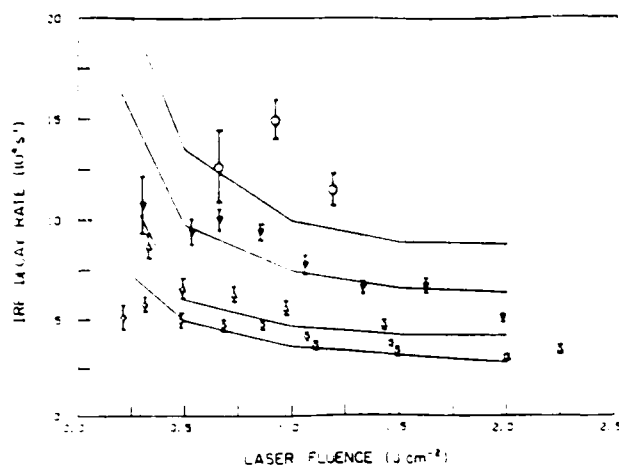


**Figure 4.** Infrared fluorescence decay rate constants. The four solid curves are calculated by using the master equation for 9 mtorr of TFE diluted in argon: (O) 358, ( $\nabla$ ) 225, ( $\Delta$ ) 120, and ( $\diamond$ ) 81 mtorr of argon, from top to bottom. The experimental points show one standard deviation uncertainties.

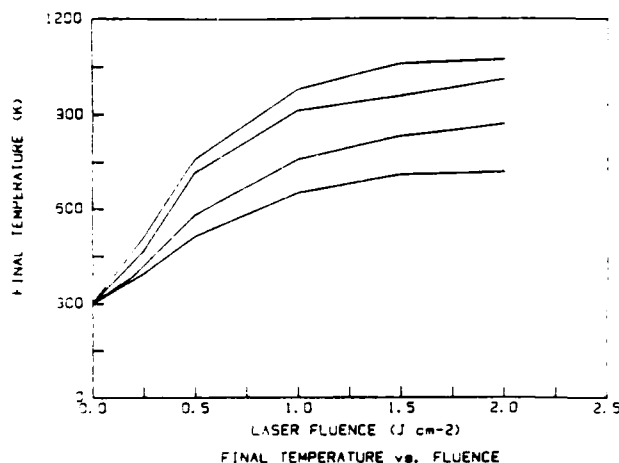


**Figure 5.** Final temperature after equilibration. Calculated by using the master equation for 9 mtorr of TFE diluted in argon. From top to bottom, the four curves correspond to 81, 120, 225, and 358 mtorr of argon.

noisy, even with extensive signal averaging. Nevertheless, a nonlinear least-squares<sup>26</sup> fit of the data beginning 6.6  $\mu$ s after the laser pulse (which occurs at 29  $\mu$ s) gives the decay constant with an uncertainty ( $\pm 1\sigma$ ) of only about 5%. This level of precision is adequate for present purposes, but it is not sufficient to detect more subtle effects, such as deviations from exact exponential decay.

To demonstrate the application of the technique, a series of experiments was performed using 9 mtorr of TFE diluted in various pressures of argon ranging from 81 to 358 mtorr, and laser fluences up to about 2  $\text{J cm}^{-2}$ . These data are presented in Table I and Figure 4 in the form of least-squares-determined decay rate constants and their associated uncertainties. Rate constants greater than about  $2 \times 10^3 \text{ s}^{-1}$  are unreliable, because of electronic response time limitations. At low fluences, the IRF intensities are very low, resulting in increased uncertainty.

For the higher pressures of argon and lower fluences, the gas temperature after equilibration is relatively low, but for high fluences and low pressures of argon, the temperature excursions are quite large, as depicted in Figure 5. Thus, the decay rate constants may reflect both dependence on internal vibrational energy and dependence on collider gas temperature. At the lower argon partial pressures, collisions between two excited TFE

**TABLE I: Infrared Fluorescence Decay Rates as a Function of Laser Fluence**

fluence, $\text{J cm}^{-2}$	decay rate, $10^4 \text{ s}^{-1}$
81 mtorr of Argon	
0.21	$5.10 \pm 0.65$
0.31	$5.74 \pm 0.41$
0.48	$4.92 \pm 0.35$
0.68	$4.68 \pm 0.28$
0.86	$4.71 \pm 0.22$
1.07	$4.09 \pm 0.22$
1.11	$3.62 \pm 0.21$
1.46	$3.67 \pm 0.17$
1.49	$3.25 \pm 0.25$
2.00	$2.95 \pm 0.18$
120 mtorr of Argon	
0.33	$8.71 \pm 0.61$
0.49	$6.57 \pm 0.49$
0.73	$6.26 \pm 0.37$
0.97	$5.57 \pm 0.35$
1.43	$4.65 \pm 0.29$
2.25	$3.36 \pm 0.20$
225 mtorr of Argon	
0.30	$10.75 \pm 1.54$
0.66	$10.00 \pm 0.54$
0.85	$9.35 \pm 0.41$
1.06	$7.69 \pm 0.49$
1.33	$6.52 \pm 0.31$
1.62	$6.52 \pm 0.36$
1.98	$4.91 \pm 0.20$
358 mtorr of Argon	
0.66	$12.60 \pm 1.75$
0.92	$14.95 \pm 0.98$
1.19	$11.40 \pm 0.81$

molecules become more probable, complicating the interpretation still further.

For all of the simulations, the functional form of  $\langle \Delta E \rangle_d$  was assumed to be the same as that used in previous work:

$$\langle \Delta E \rangle_d = \beta [T/300]^n + \gamma E \quad (1)$$

where  $\beta$ ,  $\gamma$ , and  $n$  are parameters,  $T$  is the temperature, and  $E$  is the vibrational energy.

For computer simulation and interpretation of the results, we arbitrarily assumed that the  $\langle \Delta E \rangle_d$  parameters for collisions with TFE can be approximated by those for azulene.<sup>24</sup> This assumption can be tested against experiment (see below) and it is not serious as long as deactivation by argon collisions is dominant. The assumed Lennard-Jones collision parameters are  $\sigma = 5.28 \text{ \AA}$  and  $\epsilon/K = 323$  for TFE, and  $\sigma = 3.54 \text{ \AA}$  and  $\epsilon/K = 93.3$  for argon.

For simulation of the results, the following iterative procedure was used. First, the data set for 225 mtorr added argon was simulated, assuming no dependence of  $\langle \Delta E \rangle_d$  on temperature. Here, the data set covers a wide range of fluences and the temperature excursions are relatively small due to the large amount of argon diluent. This simulation gives information mostly about the energy dependence of  $\langle \Delta E \rangle_d$ , as distinguished from the temperature dependence, because the initial population distribution of vibrationally excited TFE is controlled by varying the laser fluence and the temperature excursions are not too great. Next, the data set at 81 mtorr of added argon is simulated, including the  $\langle \Delta E \rangle_d$  temperature dependence, if necessary. Here, the temperature excursions are large, providing a test for temperature dependence. Last, we return to the first step, if necessary, and refine our fitting of the 225-mtorr data based on a  $\langle \Delta E \rangle_d$  which depends on both energy and temperature. This iterative refinement procedure results in an expression for  $\langle \Delta E \rangle_d$  that adequately fits both the 225-mtorr added argon data and that for 81-mtorr added argon. The data sets obtained at other pressures of added argon provide additional tests of the simulation.

Following the prescription given above for fitting the experimental data, it was found that an energy-independent  $\langle \Delta E \rangle_d$  simply does not fit over the entire fluence range investigated.

(26) Bevington, P. R. "Data Reduction and Error Analysis for the Physical Sciences". McGraw-Hill, New York, 1969; p 237.

However, the parameters  $\beta = 200 \text{ cm}^{-1}$  and energy dependence  $\gamma = 0.005$  gave a good fit over the entire range. In applying these same parameters to the 81-mtorr argon data set, it was found that the resulting agreement was very close to the experimental data, indicating that  $\langle \Delta E \rangle_d$  does not depend on temperature in this energy-transfer system, at least for temperatures between 400 and 1000 K. The calculated results are presented in Figure 5 as solid lines joining the calculated points. Inspection of the figure shows that all of the data sets are adequately represented by the single, temperature-independent expression:

$$\langle \Delta E \rangle_d = (200 \pm 20) + (0.005 \pm 0.002)E \quad (2)$$

where the energies are expressed in  $\text{cm}^{-1}$  and the uncertainties are estimated as the limits of acceptable simulations (future improvements in data treatment may include better means for estimating uncertainties). The simulations seem to underestimate the decay rate constants slightly, but the overall agreement between experiments and simulations is very good.

The very good agreement between simulations and experiments indicates that our starting assumption about the parameters for TFE colliding with TFE is not seriously in error. The relative importance of such collisions increases more than fourfold in going from the 358-mtorr argon data set to that for 81-mtorr added argon, but it is still small. The slight underestimate of the rate constants may, however, be due to a small underestimation of the parameters for TFE-TFE collisions.

Equation 2 indicates that the magnitude of  $\langle \Delta E \rangle_d$  is significantly smaller than expected from many unimolecular rate studies using other activated molecules.<sup>3</sup> However, investigation of 1,1,1-TFE by chemical activation<sup>27</sup> and by infrared multiphoton decomposition<sup>28</sup> studies gave  $\langle \Delta E \rangle_d = 350 \text{ cm}^{-1}$  near the reaction threshold ( $\approx 24000 \text{ cm}^{-1}$ ), in excellent agreement with the present results for 1,1,2-TFE, which give  $\langle \Delta E \rangle_d = 320 \text{ cm}^{-1}$  at the same vibrational energy. In the present study, a wider variation in excitation energy was achieved, permitting a more direct test for the energy dependence of  $\langle \Delta E \rangle_d$ .

Comparisons with other nonreactive studies are not clear-cut. The results on deactivation of azulene by argon<sup>24</sup> predict  $\langle \Delta E \rangle_d = 367 \text{ cm}^{-1}$  at  $E = 24000 \text{ cm}^{-1}$ , in fair agreement with the present study, but the energy dependence found in the azulene system ( $\gamma = 0.013$ ) is much greater than that found here. On the other hand, Troe and co-workers have found no energy dependence in any polyatomic energy-transfer system they have investigated,<sup>4,3,10</sup> but the  $\langle \Delta E \rangle_d$  values they found for argon collider gas range from about 230 to 420  $\text{cm}^{-1}$ , in general agreement with the present results.

The absence of a temperature dependence is in good agreement with other nonreactive system studies of energy transfer<sup>27,10</sup> and in clear disagreement with the investigations of Rabinovitch and

co-workers<sup>9</sup> on the reactions of isotopically substituted cyclopropanes. The reason for the disagreement has not been identified, but as new techniques are applied to energy-transfer problems, a better understanding of the process will emerge.

It should be pointed out that the heat capacities of TFE and argon are approximated in the master equation simulations by a linear dependence on temperature, whereas the actual temperature dependence is more complex. Thus, for very large temperature excursions, the temperature dependence (or lack of it) deduced from the simulations for  $\langle \Delta E \rangle_d$  may be slightly affected. The magnitude of the error introduced is related to the difference in the actual equilibrated final temperature and that calculated according to the linear heat capacity relationship and the amount of heat deposited by the absorbed laser light. For a predicted final temperature of 1000 K in a mixture of 9 mtorr of TFE and 81 mtorr of Ar, the actual temperature is about 1100 K. The error introduced is acceptably small at high temperatures and can be neglected; at lower temperatures, the errors are even smaller.

In conclusion, this demonstration shows that the technique of infrared multiphoton absorption excitation gives results in good agreement with other methods of excitation, when the population distributions have been thoroughly characterized. IR-MPA has the added advantages over other excitation methods, however, of easily controlled excitation energy (simply by changing laser fluence) and of applicability to many different classes of molecules. In principle, any technique for detection of excited molecules can be combined with IR-MPA for energy-transfer studies. For example, time-resolved ultraviolet absorbance has been used in the past to monitor the vibrational energy produced in infrared multiphoton absorption experiments,<sup>29</sup> and very recently it has been applied to collisional energy transfer in such systems.<sup>30</sup> In the present work, infrared fluorescence has been shown to be an effective method for monitoring energy transfer.

The results obtained for argon collider gas and excited 1,1,2-trifluoroethane are in reasonable accord with results obtained in other studies of other excited molecules. The results indicate a small  $\langle \Delta E \rangle_d$  energy dependence and no detectable dependence on collider gas temperature.

**Acknowledgment.** The authors gratefully acknowledge financial support from the U. S. Army Research Office. J.M.Z. acknowledges a fellowship from the Swiss Fonds National, and T.C.B. thanks Dr. K. D. King at the University of Adelaide for his support and encouragement. Many of the numerical calculations were carried out at SRI using the VAX computing facility, which was provided by a grant from the National Science Foundation. The authors are happy to acknowledge the helpful conversations with D. W. Setser, who also provided useful technical information on several molecules studied in his laboratory.

Registry No. TFE, 430-66-0; Ar, 7440-37-1.

(27) (a) Chang, H. W.; Craig, N. L.; Setser, D. W. *J. Phys. Chem.* 1972, 76, 954. (b) Marcoux, P. J.; Siefert, E. E.; Setser, D. W. *Int. J. Chem. Kinet.* 1975, 7, 473. (c) Marcoux, P. J.; Setser, D. W. *J. Phys. Chem.* 1978, 82, 97. (d) For deactivation of other fluoroethanes by gases other than argon, see Richmond, G.; Setser, D. W. *J. Phys. Chem.* 1980, 84, 2699.

(28) Jang, J. C.; Setser, D. W. *J. Phys. Chem.* 1979, 83, 2809.

(29) Knyazev, I. N.; Kudriavtsev, Yu. A.; Kuz'mina, N. P.; Letokhov, V. S.; Sarkisian, A. A. *Appl. Phys.* 1978, 17, 427.

(30) Herzog, B.; Hippler, H.; Kang, L.; Troe, J. *Chem. Phys. Lett.*, in press.

APPENDIX D.

## Sums of Quantum States for Nonseparable Degrees of Freedom: Multidimensional Monte Carlo Integration

John R. Barker

*Department of Atmospheric and Oceanic Science, Space Physics Research Laboratory, Space Research Building, The University of Michigan, Ann Arbor, Michigan 48109-2143 Received January 21, 1987*

A Monte Carlo method is described for highly efficient multidimensional integration. The sampling technique is not restricted to hyperdimensional rectangles, but it can be applied to more complicated domains. If known, the boundaries of an arbitrary integration region can be used to define the sampling domain, resulting in Monte Carlo sampling with unit efficiency. When applied to calculating sums of states, the method in principle can include all molecular degrees of freedom, coupled in any fashion. The Monte Carlo integration method is demonstrated by calculating the vibrational sums of bound states for  $\text{H}_2\text{O}$  and  $\text{CH}_2\text{O}$ , based on their spectroscopic constants, including all diagonal and off-diagonal anharmonicities. The method was found to be highly efficient and practical for calculations involving moderate-sized molecules, even for vibrational energies substantially above the dissociation energy. The results show that inclusion of the off-diagonal anharmonicities produces a significant increase in the calculated sum of vibrational states.

### Introduction

Sums and densities of molecular states are needed in calculations of RRKM unimolecular rate constants, energy-transfer systems, infrared multiphoton absorption, radiationless transitions, and any system in which detailed balance is invoked. Thus, methods are needed for calculating the sums and densities of molecular states, regardless of the nature of the degrees of freedom and whether they are coupled.

In vibrationally and rotationally excited molecules, the degrees of freedom are strongly coupled, affecting the dynamics of intramolecular vibrational relaxation. At high energies, near and above reaction thresholds, the coupling can be very large, seriously affecting the sums and densities of states. In fact, the "transition state"—with frequencies different from the ground-state molecule—is a device that is used to account for the effects of coupling.

The Beyer-Swinehart algorithm<sup>1</sup> (and its extensions by Stein and Rabinovitch<sup>2</sup>) revolutionized calculations of molecular-state sums ( $G(E)$ ) and densities ( $\rho(E) = dG(E)/dE$ ), since its high efficiency made exact counts of states practical for most molecules. Despite its great usefulness, an unfortunate limitation of this algorithm is that it can be applied only to separable degrees of freedom. In principle, the method of steepest descents and other methods based on approximate inversion of the partition function<sup>3</sup> can be used for nonseparable degrees of freedom, but the partition functions are not known, making this approach impractical.

Several groups have applied Monte Carlo techniques to the problem of calculating  $G(E)$  for nonseparable degrees of freedom. Monte Carlo techniques are attractive, because they do not depend on the particular degrees of freedom or its coupling.<sup>4</sup> In a recent publication, Doll showed how the semiclassical  $G(E)$  for a classical Morse oscillator can be obtained by application of "crude" Monte Carlo techniques;<sup>5</sup> nonseparable potentials can be treated by the same method. Farantos, Murrell, and Hajduk applied stratified Monte Carlo sampling to calculate semiclassical  $G(E)$ 's and  $\rho(E)$ 's for coupled vibrational and rotational degrees of freedom.<sup>6</sup> In developing a Monte Carlo version of transition-state theory, Viswanathan, Raff, and Thompson<sup>7</sup> developing an interesting Metropolis-Markov chain technique for calculating densities of states for coupled, anharmonic potentials.

As pointed out by Farantos et al.,<sup>6</sup> much of the research involving Monte Carlo methods is motivated by the need to increase efficiency. The stratified sampling technique they used (developed by Friedman and Wright<sup>8</sup>) is relatively efficient and is available as a "canned" computer code, but it appears to be cumbersome. Moreover, the "strata" are constrained to be hyperrectangles, even when other geometries would give greater efficiency.

In the present paper, we describe a relatively simple Monte Carlo sampling technique that gives unbiased estimates and which has a high efficiency. Moreover, the sampling technique can be easily applied to any arbitrary sampling geometry. This feature may enable development of stratified sampling schemes and importance sampling schemes<sup>9,10</sup> that capitalize on the optimum geometry of particular problems. Even without such refinements, however, the method is practical for sums of states calculations on moderate-sized molecules.

In testing the sampling technique, quantum  $G(E)$  was calculated from recent spectroscopic data for the (nonseparable) vibrational modes of water<sup>11</sup> and of formaldehyde.<sup>12</sup> The results show that the coupling among the vibrations can significantly increase  $G(E)$  at moderate energies, compared to the  $G(E)$  calculated for separable anharmonic vibrations. This result is particularly important in comparisons of transition-state theory rate constants calculated from potential energy surfaces, when tunneling (or some other effect) is invoked to explain differences from experiments or from the results of other calculations.

### Theory

The sampling algorithm described below can be applied to continuous variables, discrete variables, or a combination of the two. Since the motivation of the present work is the calculation of quantum sums of states, the descriptions will be based on discrete random variables (quantum numbers), but the approach is easily generalized to any multiple-dimensional integral or sum.

In "crude" Monte Carlo<sup>9</sup> sampling, each random variable is sampled independently and uniformly, resulting in a uniform distribution of sample points throughout the hyperrectangle defined by the respective ranges of the independent variables. The variable ranges are chosen so that the integration region lies entirely within the sampling hyperrectangle. If the sample points fall within the integration region, they are counted successes and the integral

(1) Beyer, T.; Swinehart, D. F. *Commun. ACM* 1973, 16, 379.  
(2) Stein, S. E.; Rabinovitch, B. S. *J. Chem. Phys.* 1973, 58, 2438.  
(3) Forst, W. *Theory of Unimolecular Reactions*; Academic: New York, 1973, p 104.  
(4) Noid, D. W.; Koszykowski, M. L.; Tabor, M.; Marcus, R. A. *J. Chem. Phys.* 1980, 72, 6169.  
(5) Doll, J. D. *Chem. Phys. Lett.* 1980, 72, 139.  
(6) Farantos, S. C.; Murrell, J. N.; Hajduk, J. C. *Chem. Phys.* 1982, 68, 199.  
(7) Viswanathan, R.; Raff, L. M.; Thompson, D. L. *J. Chem. Phys.* 1984, 91, 428.

(8) Friedman, J. H.; Wright, M. H. *ACM Trans. Math. Software* 1981, 7, 76.  
(9) Hammersley, J. M.; Handscomb, D. C. *Monte Carlo Methods*; Chapman and Hall: London, 1964.  
(10) Rubinstein, R. Y. *Simulation and the Monte Carlo Method*; Wiley: New York, 1981.  
(11) Benedict, W. S.; Gailar, N.; Plyler, E. K. *J. Chem. Phys.* 1956, 24, 1139.  
(12) Reisner, D. E.; Field, R. W.; Kinsey, J. L.; Dai, H.-L. *J. Chem. Phys.* 1984, 80, 5968.

$S$  is given by the sampling volume ( $V_s$ ) multiplied by the ratio of successes ( $n$ ) to trials ( $N$ ):

$$S = V_s n / N \quad (1)$$

If the integration region is not a hyperrectangle and of about the same size as  $V_s$ , the efficiency (here defined as  $\epsilon = n/N$ ) can be very low, resulting in poor precision of the Monte Carlo method. For multidimensional integrals, this poor efficiency can cripple the approach, since astronomical numbers of trials must be calculated for high-precision results.

To improve the efficiency of the method, numerous "variance reduction" methods have been developed.<sup>8-10</sup> The approach adopted here is to choose a sampling domain that resembles the integration region as closely as possible; in the limit, the sampling domain may be identical with the integration region. In general, the ideal sampling domain is not a hyperrectangle of independent variables but a more complicated shape; the sampling range of a given variable will depend on values already selected for the other variables. Moreover, the distribution of sample points is not uniform throughout the sampling domain, necessitating the calculation of appropriate weighting factors.

For Monte Carlo integration, consider a multidimensional sampling volume  $V_s$  defined in a space of discrete variables (e.g., quantum states). The  $g$ th sample point, or cell, is designated by a complete set of variable values (quantum numbers). Equation 1, for any type of sampling, can be written in terms of the total  $G$  cells and weighted sums over  $f(g)N_g$  and  $N_g$  where  $f(g)$  and  $N_g$  are the value of the integrand and the numbers of trials performed at the  $g$ th cell

$$S = V_s \sum_g f(g) N_g / \sum_g N_g \quad (2)$$

where the summations extend over the  $G$  cells. Equation 2 can be used with any type of sampling to obtain estimates of  $S$ . However, the sampling volume  $V_s$  must be known, as well as the weight function  $w_g$ . For complicated sampling domain boundaries (as in sums of states calculations),  $V_s$  may not be known.

For the special case of uniform sampling, the sampling domain is a hyperrectangle of volume  $V_0$  containing  $G (= \alpha V_0)$  cells and the weight function is a constant

$$w_0 = 1/G = \lim_{N \rightarrow \infty} N_g / N \quad (3)$$

where  $N = \sum N_g$  is the total number of trials and  $w_0$  is the weighting function.

For uniform sampling, eq 2 is an unbiased estimator for  $S$ .<sup>8</sup> Now suppose that we employ weighted sampling with normalized weight function  $w_g$  in a new sampling volume  $V_s$  that is completely enclosed within  $V_0$ ; the new sampling domain contains  $G'$  cells (of the same size as in  $V_0$ ), but we do not, in general, know the value of either  $V_s$  or  $G'$ . The weight function can be expressed as the ratio of the number of trials  $N_g'$  at the  $g$ th cell divided by the total of trials  $N'$  made using the weighted sampling technique:

$$w_g = \lim_{N' \rightarrow \infty} N_g' / N' \quad (4)$$

Using this identity, we can connect the number of trials at the  $g$ th cell that are made using uniform sampling to the number that are made using the weighted sampling method:

$$\lim_{N \rightarrow \infty} f(g) N_g / N = (w_0 / w_g) (f(g) N_g' / N') \quad (5a)$$

$$\lim_{N \rightarrow \infty} N_g / N = (w_0 / w_g) (N_g' / N') \quad (5b)$$

For complicated integrands, eq 5a must be used, but for simple determinations of volume, the function  $f(g)$  equals unity inside the volume and zero outside the volume. Thus, in eq 5b we can write  $n_g'$  in place of  $f(g)N_g'$  where  $n_g'$  is the number of successes obtained with weighted sampling at the  $g$ th cell. These equations are used to express the numerator of eq 2 in terms of  $n_g'$  and the denominator in terms of  $N' = w_0 \sum (N_g' / w_g)$ , from eq 5

$$S = w_0 V_0 N'^{-1} \sum f(g) N_g' / w_g \quad (6a)$$

$$= w_0 V_0 N'^{-1} \sum n_g' / w_g \quad (6b)$$

where the summations extend over the  $G'$  cells. Note that the number of cells in the hyperrectangle is  $G = \alpha V_0$  and  $w_0 = 1/G$ . Thus,  $w_0 V_0 = 1/\alpha$ , and we obtain an expression for the integral that does not explicitly depend on knowledge of  $V_s$

$$S = (\alpha N')^{-1} \sum f(g) N_g' / w_g \quad (7a)$$

$$S = (\alpha N')^{-1} \sum n_g' / w_g \quad (7b)$$

Note that the summations in eq 6 and 7 extend only over the  $G'$  cells contained in the new sampling domain, because there are no trials outside that region. Of course, not all cells will be sampled, and so the sum extends only over the sampled cells. Thus, we do not need to know the value of  $G'$ .

The precision of the Monte Carlo estimator is monitored by the usual expression<sup>9</sup> for the estimated error of the mean

$$\sigma^2 = |N'(N' - 1)|^{-1} \sum (w_g f(g) N_g' - S)^2 \quad (8)$$

where  $\sigma$  is the standard deviation of  $S$ .

Equation 7 is completely general, and it also applies to sampling in continuous variables. For discrete variables, the proportionality constant  $\alpha$  is conveniently set to unity, so that the number of cells in the hyperrectangle is numerically equal to  $V_0$ . Equation 7a is the general result, while eq 7b is specifically appropriate for calculating volumes in multidimensional space.

Note that eq 7b can be used to find  $V_s$ , the volume of the weighted sampling domain, if the boundaries of the volume are known and if  $w_g$  is known. This fact can be particularly useful in calculating unknown volumes in multidimensional space when only the volume boundaries are known, since the sampling domain boundaries can be set equal to the boundaries of the unknown volume; every trial will be a success, leading to unit efficiency. Nonetheless, many trials must still be made, because the limits expressed in eq 4 and 5 are required.

To utilize eq 7, we need to define a normalized distribution of sample points, from which  $w_g$  can be calculated. A distribution of sample points that can be tailored to arbitrary sampling geometries is presented in the next section.

### Sample Point Distribution and Sampling Algorithm

The following algorithm defines a distribution of sample points constrained to an arbitrary sampling domain.

1. Choose an appropriate sampling domain in  $s$ -dimensional space that completely encloses the integration region; express it as

$$B = F(u_1, u_2, \dots, u_s) \quad (9)$$

where eq 9 defines the  $(s-1)$ -dimensional boundary surface in terms of the variables  $u_1, \dots, u_s$ .

2. Starting with all  $u_i$  at their minimum values, calculate the maximum value of  $u_1$  consistent with eq 9. The range of  $u_1$  is then given by

$$R_1 = u_{1, \max} - u_{1, \min} \quad (\text{continuous variables})$$

$$R_1 = 1 + u_{1, \max} - u_{1, \min} \quad (\text{discrete variables})$$

3. Use a uniformly distributed random number  $U$  ( $0 \leq U < 1$ ) to select a value of  $u_1$  from the range  $R_1$

$$u_1 = UR_1 + u_{1, \min} \quad (10)$$

(note: truncate  $u_1$  for integer variables.)

4. Repeat steps 2 and 3 for each  $u_i$ , but in eq 9, use the values already selected for the preceding variables. Continue this process until values for all variables have been selected, consistent with eq 9. This will result in the selection of a sample point within the sampling domain defined by eq 9. Note that the range of the  $i$ th variable is conditional with respect to all variable values previously selected.

5. Calculate the weighting factor,  $w_g$ , for sample point  $g$

$$w_g = \prod_{i=1}^s R_i^{-1} \quad (11)$$

where  $R_i$  is the range of the  $i$ th variable.

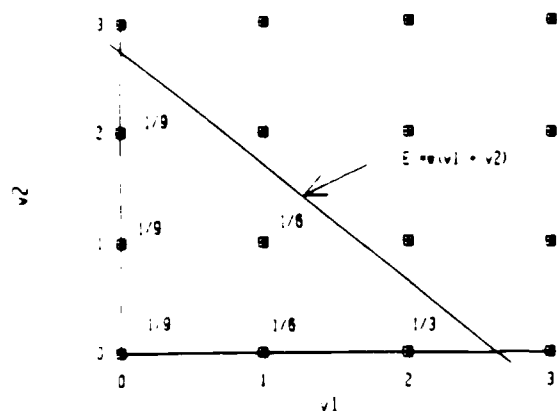


Figure 1. Two-dimensional sampling volume

6. Determine the value of  $f(g)$  (or whether the trial is a success or a failure) and add the results to the summations in eq 7.

7. Test to determine whether the maximum number of trials or a criterion for precision (e.g., relative standard deviation) has been reached; if so, terminate the calculation.

8. Although not strictly required, the order of selection of the variables can be shuffled to eliminate the variable weighting that depends on their order of selection (see below).

9. Return to step 1 and initiate a new trial.

The distribution of sample points that results from this algorithm is normalized but not uniform. Furthermore, the variables are weighted depending on the order in which they are selected. This is most easily demonstrated for discrete variables, e.g.,  $v_i$  corresponding to vibrational quantum numbers.

For example, consider a molecule containing two separable vibrational modes

$$E = v_1\omega_1 + v_2\omega_2 \quad (12)$$

where  $E$  is the vibrational energy in excess of the zero-point energy and the  $\omega_i$ 's are the harmonic oscillator energy level spacings. This equation defines the two-dimensional sampling domain shown in Figure 1. The sum of vibrational states is the area enclosed by the diagonal line and the two axes. (For simplicity, Figure 1 depicts the case when  $\omega_1 = \omega_2$ , but this condition is not necessary, in general.) (Note when anharmonicities are included, the straight diagonal boundary is replaced by a curved line, making this problem much more difficult.)

The sampling algorithm and weighting factor reflect the probability of selecting particular pairs of variables. In Figure 1, energy  $E$  corresponds to up to two quanta in either of the two modes or one quantum in each mode. Selecting  $v_1$  first, the range  $R_1 = 3$  (i.e.,  $v_1 = 0, 1, 2$ ); if the selected value is  $v_1 = 0$ , then  $R_2 = 3$  (i.e.,  $v_2 = 0, 1, 2$ ), but if  $v_1 = 1$  or  $2$ , then  $R_2 = 2$  or  $1$ , respectively. Thus, the probability of choosing a particular pair of values is  $(R_1 R_2)^{-1}$ , as noted in Figure 1; this probability is just the weighting factor  $w_f$ . Note that the weighting factor is normalized:

$$\sum_{f=1}^G w_f = 1 \quad (13)$$

As shown in Figure 1, the distribution of sample points is not uniform. The algorithm tends to weight the higher energies more heavily than the lower energies. Variables chosen earlier in the sequence are more often selected with higher quantum numbers than those selected later. This causes no problems for sufficient numbers of trials, but convergence appears to be faster when the selection order is shuffled between trials. Shuffling eliminates the weighting due to selection order, but the higher energy points are still selected more often than the low-energy points. This constitutes a fortuitous "importance sampling" effect that is desirable in calculating sums of states, where the sum varies more rapidly at high energies.

The computational speed of this Monte Carlo method depends on the efficiency  $\epsilon$ , which can equal unity, and on the computation

of the boundaries, weights, and integrand. This algorithm calculates the weighting factors "on the fly" and without knowing  $V_i$ , improving the efficiency of the method, since weights are calculated only for the points actually sampled. The necessity of calculating the boundaries of  $V_i$  from eq 9 costs some computational labor, and thus simple boundaries are desirable. Other factors can also affect computational speed. For example, the cost of shuffling the ordering of the variables must be weighed against the cost of simply running more trials. We have not explored all of these discretionary factors but have arbitrarily chosen to shuffle the ordering after every trial.

Sums of states for individual symmetry species are useful for various purposes. Several authors have described methods for calculating the sums of states for individual symmetry species in molecules with separable degrees of freedom.<sup>13-15</sup> For nonseparable degrees of freedom, the same symmetry species apply,<sup>16</sup> but the sums of states will be affected by the coupling. The present approach lends itself naturally to calculating sums of states for nonseparable degrees of freedom, because complete sets of quantum numbers are selected in each trial. The symmetry species of each vibrational state can be determined by application of Tisza's rules<sup>17</sup> or the simplification described by Lederman, Runnels, and Marcus.<sup>13</sup> The number of successes for each symmetry species can be stored separately to give the sums of states of each type.

#### Sampling Domain for Coupled Vibrational States

For nonseparable anharmonic vibrations, the conventional expression for the vibrational energy in excess of the zero-point energy is

$$E = \sum_{i=1}^f v_i(\omega_i + X_{ii}v_i) + \sum_{i=1}^f \sum_{j>i}^f X_{ij}v_i v_j \quad (14)$$

where  $\omega_i$  are the frequencies and  $X_{ij}$  are the anharmonicities. This equation defines the boundary of the integration region for bound states, and it can be used to define the boundary of the sampling region. A relatively simple calculated boundary is obtained if only the first summation term is retained: this corresponds to separable vibrations. When the off-diagonal anharmonicities are small, the "separable" boundary closely approximates the actual boundary and it is a good choice, but when the couplings are larger, the full equation can be used (see below). To ensure that the integration region is contained entirely within this sampling domain, the boundary is calculated for the energy  $E_b = \beta E$ , where  $\beta \geq 1$ . For anharmonic vibrations, the magnitude of  $\beta$  will be of the order of unity, if  $X_{ii} \approx X_{ij}$ .

The most accurate boundary can be calculated during the quantum number selection process by taking into account the quantum numbers already selected and including the off-diagonal anharmonicities. This is done by using eq 14 to calculate the energy already assigned to the first  $(k-1)$  vibrations and subtracting this energy from  $E_b = \beta E$ . The remaining energy is then available for assignment to the  $k$ th and subsequent modes, as follows.

If the unassigned energy  $E_u$  is greater than the dissociation energy of the  $k$ th mode, the maximum quantum number (the dissociation limit) is

$$v_{k,\max} = v_{k,D} = -|\omega_k + \sum_{i>k}^f X_{ik}v_i| / (2X_{kk}) \quad (15)$$

If, on the other hand,  $E_u$  is less than the dissociation energy,  $v_{k,\max}$  is given by

$$v_{k,\max} = v_{k,D} \{1 - [1 + E_u / (X_{kk}^2 v_{k,D}^2)]^{-1/2}\} \quad (16)$$

(13) Lederman, S. M.; Runnels, J. H.; Marcus, R. A. *J. Phys. Chem.* 1983, 97, 4364.

(14) Sinha, A.; Kinsey, J. L. *J. Chem. Phys.* 1984, 80, 2029.

(15) Quack, M. *J. Chem. Phys.* 1985, 82, 3277.

(16) Wilson, E. B.; Decius, J. C.; Cross, P. C. *Molecular Vibrations*. McGraw-Hill: New York, 1955; p 151.

(17) Tisza, L. *Z. Phys.* 1933, 92, 48; also, ref 15, p 331 ff.

END

DATE

FILM

3-88

DTIC